University of Heidelberg & University of Mainz

Diploma Thesis

Measurements and Procedures for the Construction and Characterization of Ultra-Cold Neutron Guides.

Author:

Leonard Göltl-Simmenauer

Supervisors:

Prof. Johanna Stachel

Prof. Jens V. Kratz

20th November 2008

Abstract

This work investigates different measurement principles to characterize ultra-cold neutron guides. UCN transmission was studied employing the time-of-flight method and an alternative measurement principle - using pre-storage - was considered and tested. Furthermore, the UCN transmission of aluminum foils was investigated. The work also includes a detailed description of several pieces of hardware - one of which was built as part of this work - needed for the experiments.

Acknowledgements

First of all I want to mention that this work would not have been possible without my parents for obvious reasons, thank you for everything you have done!

I had the great opportunity to work on my thesis without any financial worries on my mind because I was enjoying a very generous scholarship from the Gerhard C. Starck Foundation[1] in Germany. I am very thankful for the years of support provided by the foundation. Special thanks go to Inge Frey.

Now for the scientific support I want to mention the UCN group at PSI, namely: Fritz Burri****, Manfred Daum[a], Reinhold Hennck, Bernhard Lauss*, Malgorzata Kasprzak, Klaus Kirch[a], Andreas Knecht, Marcin Kuzniak, Michael Meier**, Alexander Mtchedlishvili, Gerd Petzoldt and Geza Zsigmond***.

*My supervisor, boss and colleague. Thank you for the (im)patience and the endless corrections.

a: Thank you for the advice and corrections.

**Our group technician who made it possible, that I could work in the workshop without significant losses or injuries.

***Who showed great patience with me, explaining theoretical background and math so that even I could understand it!

****Who let me use his electronics workbench although I would always make a mess out of it.

I also want to mention Thorsten Lauer and Iouri Sobolev, from the Mainz UCN group, who operate the UCN source. The Mainz UCN diploma students were also a great help, not only during the experiments!

Special thanks go to the supervising professors, Dr. Jens V. Kratz, supervising me from Mainz and Dr. Johanna Stachel, supervising me from Heidelberg and allowing me to take the great opportunity of finishing my studies in Switzerland.

Contents

Chapter 1

Introduction

1.1 Motivation

At Paul Scherrer Institute (PSI) in Villigen (CH), construction of the world-wide most powerful ultra-cold neutron source is ongoing. The yield of ultra-cold neutrons (UCN) from that source is going to exceed the currently strongest UCN source, at the Institut Laue Langevin (ILL) in Grenoble, France, by one to two orders of magnitude [1, 2]. The opportunity to measure fundamental physics parameters of the neutron, i.e., the neutron lifetime or its electric dipole moment, with unprecedented precision, highly motivates the construction of such an intense UCN source.

The neutrons will be produced via nuclear spallation. This process, in which a target nucleus is hit by a projectile particle, leads to the expulsion of neutrons, protons and nuclear fragments. At PSI, the projectiles are protons with an energy of 590 MeV and an intensity of more than 2 mA. The target mainly consists of lead [3]. The source is skeched in Fig. 1.1, (p.5).

Nuclear spallation leads to a high level of radiation, hence the source is surrounded by a large biological shielding, typically a wall of iron and

concrete. The total thickness of this shielding is $\sim$5 m. The spallation neutrons are thermalized in heavy water surrounding the solid D_2 converter from which UCN enter a storage volume. In order to provide UCN to experiments, neutron guides have to be installed, which guide the neutrons from the UCN storage volume through the biological shield as efficiently as possible. The goal of this thesis is to experimentally determine properties of such UCN guides and extract parameters describing the UCN transport.

1.2   Ultra-Cold Neutrons

The neutron is one of the two particles atomic nuclei are made of. In stable nuclei, the neutron is a stable particle, but if the neutron is separated from the nucleus, it has a lifetime of about 900 seconds until it decays via weak interaction:

$$\text{n} \rightarrow p + e^- + \bar{\nu}_e \tag{1.1}$$

The term "ultra-cold" refers to the low kinetic energy of neutrons in terms of a temperature. If neutrons, treated as an ideal gas in thermal equilibrium, the thermal energy is:

$$\text{E}_{\text{th}} \; = \; \frac{3}{2}\text{k T} \tag{1.2}$$

with an individual kinetic energy:

$$\text{E}_{\text{kin}} \; = \; \frac{1}{2}\text{m}_{\text{n}}\text{v}^2. \tag{1.3}$$

Here m_{n} is the neutron mass, v the neutron velocity, k the Boltzman constant and T the temperature of the "neutron gas".

One thus obtains the usual relation between velocity and temperature:

$$v = \sqrt{\frac{3k\ T}{m_n}} \tag{1.4}$$

Free neutrons can be categorized according to their kinetic energies.

- The most energetic neutrons, called fast neutrons, are those, that emerge from nuclear reactions, meaning they have energies of some MeV. These neutrons are not in thermal equilibrium.

- Neutrons that are moderated by a medium at room temperature are either called epithermal (i.e., they still have more energy than the surrounding particles), or once they are in thermal equilibrium with the moderator they are called thermal neutrons (E~0.025 eV or v~2200m·s^{-1}).

- Cold neutrons are those in thermal equilibrium with a cold moderator, liquid deuterium for example at $T \approx 25$ K.

- The definition of ultra-cold neutrons is given as those neutrons that can be stored in a material trap. This is possible for UCN with energies ≤300neV, equivalent to a temperature of ~3 mK. However, these UCN are not in thermal equilibrium with their environment.

Such slow neutrons do not pass through a wall, if their energy is lower than the material optical potential of the wall. Instead of interacting with a single nucleus, the neutrons interact with an effective potential, created by the sum of the single nuclei, which is sometimes termed Fermi potential V_F. If the energies of the neutrons exceed the Fermi potential they will be transmitted through the surface. To be exact, this has to be calculated within quantum mechanics. The theory for scattering of neutrons will be addressed in Chapter 2.

UCN can be produced in several different ways. One way is to guide thermal neutrons into a solid D_2 crystal in which the neutrons undergo phonon scattering, i.e., they are down-scattered[1] to a kinetic energy in the nanoelectronvolt range [4]. That approach is used for the PSI and the Mainz UCN sources. A very different approach is realized at the ILL where cold neutrons are produced in a liquid deuterium source. These neutrons are guided first vertically, losing energy to gravity, then in a bent guide that leads them to the UCN turbine[2] (see Fig. A1, p. ii). Here the neutrons are decelerated mechanically by reflections on the turbine blades spinning in the direction of the UCN flight path.

1.3   The PSI UCN Source

At the PSI source, ultra-cold neutrons will be produced in the following way: Protons from the 590 MeV PSI ring cyclotron with a continuous wave intensity of $I_p \geq 2$ mA, i.e., at a power of more than 1.2 MW, hit a spallation target made of lead-filled zircalloy tubes [3, 6] which is located in the middle of a heavy water moderator. The proton beam is pulsed by deflecting the beam with a fast kicker magnet [7] into a beam line leading to the UCN source. The duty cycle is 1 %, e.g., the pulse duration is 8 s every 800 s. The protons produce mainly fast and epithermal neutrons upon impact. The emerging neutrons are thermalized in the heavy water moderator and may enter a solid deuterium crystal, which has a temperature of about 6 K. The size (30 dm^3) and thickness of the crystal ($\sim$15 cm) reflect the mean free path of a UCN in solid deuterium and will be optimized to obtain the highest yield of ultra-cold neutrons emerging from the top of the crystal

---

[1]Down-scattering means that a part of the kinetic energy of a neutron is transferred to a lattice vibration of the D_2 crystal (phonon), hence the neutron is slowed down.

[2]UCN source invented by Albert Steyerl at TU Munich [5]

through Monte-Carlo calculations and experimentally. Inside the crystal, the neutrons are moderated to the cold region and finally down-scattered to become ultra-cold. The UCN are guided upwards to a DLC[3] coated storage volume. UCN guides lead from there to two experiment zones. These guides can be opened and closed on demand.
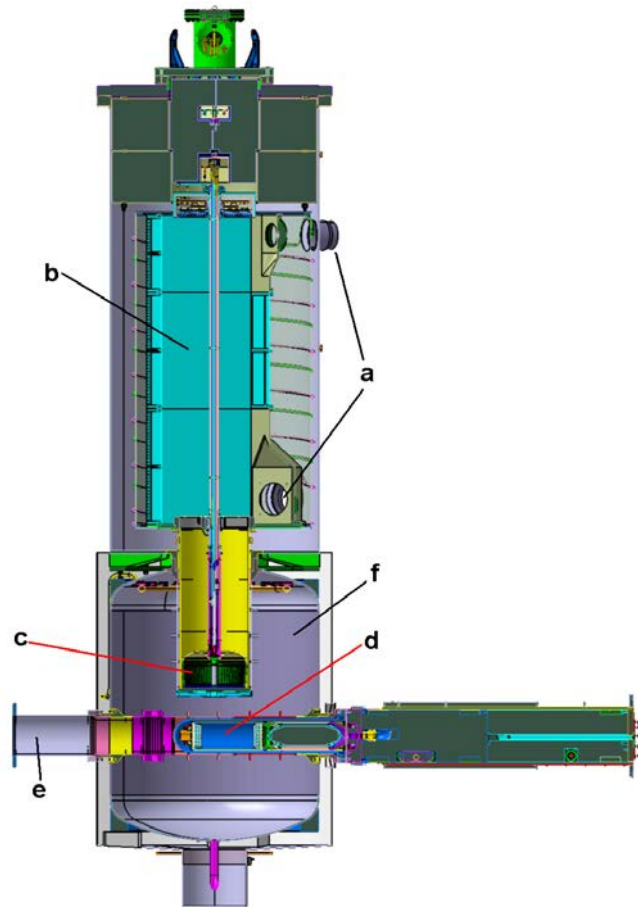
Figure 1.1: The UCN source planned at the Paul Scherrer Institute in Villigen, Switzerland. a) Neutron guide ports, b) UCN storage volume, c) D_2 crystal (UCN converter), d) lead target, e) proton beam tube, f) heavy water moderator. This setup is placed inside the biological shield.

---

[3]DLC - Diamond-Like Carbon, carbon with a high amount of sp^3 hybridized atoms and a high material potential ($\sim$250 neV).
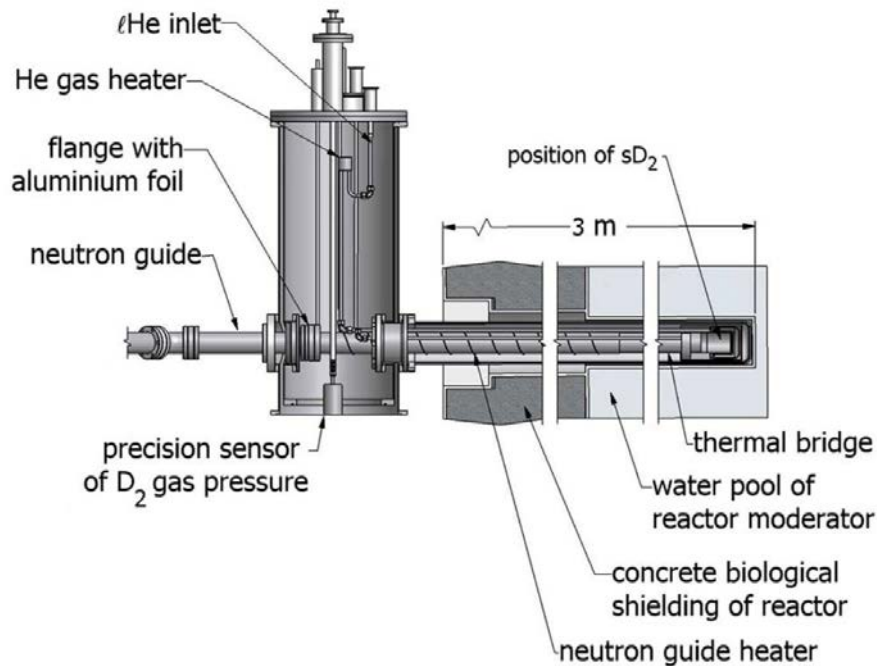
Figure 1.2: Schematic of the UCN source at the TRIGA reactor in Mainz [8].

1.4 The Mainz UCN Source

The Mainz UCN source [8, 9] uses the TRIGA Mark II reactor (see below) in the Institut für Kernchemie. Thermal neutrons that were moderated in the fuel elements are converted to UCN in a D_2 crystal located in a cryostat, inserted in beam tube C of the TRIGA reactor. The D_2 crystal is obtained by freezing out several mol ($\sim$7 mol) of D_2 at $\sim$5 K, via liquid He cooling. In [8] details of the source optimization are discussed. One important conclusion is that thermal cycling[4] of the sD_2 increases the yield of UCN from the source. Also [8] discusses the option of different pre-moderators positioned around the nose of the cryostat. Figure 1.2 shows a schematic of the UCN source with the gas handling system.

---

[4]Heating and cooling the cryostat between 5 and 13 K.

1.4.1 The TRIGA Reactor in Mainz

TRIGA stands for Training, Research, Isotopes, General Atomic. It is a class of small nuclear reactor built by the company General Atomics[5]. There is a "TRIGA Mark II" installed at the Institut für Kernchemie in Mainz [18, 19]. The UCN source in Mainz uses neutrons produced in that reactor.

The TRIGA reactors are very safe due to the design of their fuel rods. By combining U-235 with zirconium-hydride, the rods have a prompt negative temperature coefficient in the reactivity, i.e., they are intrinsically safe, even if the control rods are rapidly removed.

The TRIGA Mark II can be operated in two different modi, in the continuous mode and in the pulsed mode. In continuous mode, the reactor has a thermal power of 100 kW, in pulsed mode it can reach up to 250 MW (pulse maximum). Continuous mode means the reactor is producing a constant power (100 kW) and the UCN source, therefore, produces a constant UCN flux. This mode is used for measurements with the chopper. The pulsed mode produces a big number of neutrons in short time (< 1 s), it can thus be used for experiments involving UCN storage. This pulse is obtained by bringing the reactor to criticality in a low-power (50 W) steady state and then shooting the pulse rod out of the reactor core and later allowing it to fall back in place. The propulsion is achieved with compressed air.

In principle, a TOF measurement can be performed both in the pulsed or in steady state mode of the reactor. In the pulsed mode, the minimal overall length of the flight path is from the geometrical layout (shielding, cryostat, etc., cf. [9]) more than 6 m. In such a long UCN guide, part of the

---

[5]General Atomics, 3550 General Atomics Court, San Diego, CA 92121-1122, `www.ga.com`

neutrons are repeatedly diffusely scattered back and forth and the neutron guide acts also as a neutron storage chamber. This leads to a delay of these scattered neutrons in reaching the detector apparently at a lower velocity. In the steady state mode, using a chopper for the TOF information, the TOF path length can be chosen to be much shorter.

1.5 Experimental Characterization of UCN Guides

The most important ways to test UCN guides are via UCN transmission and UCN storage measurements. These two types of measurements should be done for every UCN guide to characterize it before the installation at the source. Besides the obvious need to test every component of a complex system before mounting, to prevent single component failure, there is one other reason in case of the UCN guides. Once the source is operating, the guide materials will be quickly radio-activated and a replacement of a guide is a money and time consuming effort.

- **Transmission experiments:** In transmission experiments, one measures neutron count rates in two specific setups. Measurement 1 is done with a defined setup without the test guide (i.e., the tube that is to be characterized), then for measurement 2, the test guide is mounted onto the previously used defined setup and the neutron count rate is measured again, see Figs. 4.1 and 4.2 for schematics. The transmission of the UCN guide is defined as the number of UCN exiting the test guide divided by the number of UCN entering the test guide.

- **Storage experiments:** In storage experiments, the definition of UCN is used, namely that UCN are those neutrons, that can be trapped in a material bottle. The trap, or in our case the guide, is filled

with UCN for a given time, then closed and left closed for a certain trapping time. After the trapping time, the trap is reopened and the remaining UCN are counted. This experiment is repeated for different trapping times and the number of UCN is recorded vs. the trapping time. The exponential decay of the UCN with the trapping time can be described by a "storage time" constant which provides characteristics of the observed test guide. See Fig. 1.3 for a sketch.

Both types of experiments are described in more detail in chapters 4 and 7.
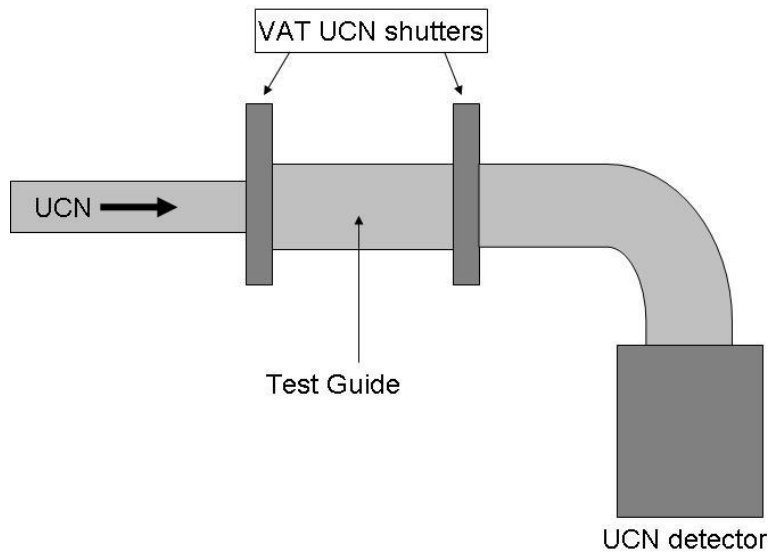
Figure 1.3: Schematics of the setup for the storage experiments: The test guide is mounted in-between shutters that allow to open or close the trap remotely. The neutron detector is placed after a 90° bend below the experiment.

Chapter 2

Theoretical Considerations

2.1 Interactions of Ultra-Cold Neutrons and their Relevance to this Work

This chapter provides an overview of how the influence of the four fundamental forces of nature on the neutrons affect the measurements of storage time and UCN transmission. The following description of the interactions and the introduction of the Fermi potential are written along the lines of the reasoning given in [10].

2.1.1 Gravity

The neutron is a particle with a mass of 939.565 $\frac{\text{MeV}}{\text{c}^2}$, which corresponds to $1.674 \cdot 10^{-27}$ kg. The gravitational attraction is obviously the same for every neutron, but in comparison with their kinetic energy, negligible for fast and thermal neutrons. On cold or ultra-cold neutrons, however, the effect is of relevant scale. The gravitational potential is given by:

$$V_{\text{g}} \;=\; m_{\text{n}} \cdot \; \text{g} \cdot \; \text{h} \tag{2.1}$$

10

Using the earths gravitational attraction (i.e., g = 9.81 m·s^{-2}) and a difference in height h, one obtains a potential difference of $\Delta V_{\mathrm{g}} = 102$ neV·m^{-1}. Gravity is used in our experiments to shift the velocities of UCN up- or downwards.

In our experiments at the TRIGA[1] reactor in Mainz, we gained a factor of 2 in UCN rate by raising the setup by half a meter with respect to the UCN output of the source [9]. This shifted the maximum of the velocity spectrum to the UCN regime.

2.1.2 Electromagnetic Interaction

The neutron has a spin of $\frac{\hbar}{2}$, thus it is a fermion. This spin results in a magnetic moment μ which interacts with magnetic fields and is described by the potential:

$$V \quad = \quad -\overrightarrow{\mu} \cdot \overrightarrow{B} \tag{2.2}$$

$$V \quad = \quad \pm 60 \tfrac{\mathrm{neV}}{\mathrm{T}} \cdot B. \tag{2.3}$$

Furthermore, a force is exerted on the neutron in an inhomogeneous magnetic field:

$$\overrightarrow{F_m} \quad = \quad \bigtriangledown \, [\overrightarrow{\mu} \cdot \overrightarrow{B}]. \tag{2.4}$$

This magnetic force can be used to trap the neutrons in a magnetic bottle or to select one of the two spin states. The magnetic interaction is especially relevant for experiments using polarized neutrons.

---

[1]$\underline{\mathrm{T}}$raining, $\underline{\mathrm{R}}$esearch, $\underline{\mathrm{I}}$sotopes, $\underline{\mathrm{G}}$eneral $\underline{\mathrm{A}}$tomics; an acronym for an atomic research reactor built by General Atomics. The research reactor used in this thesis is installed at the Institute for Nuclear Chemistry in Mainz.

2.1.3 Weak Interaction

The free neutron decays via the β-decay as follows:

$$\text{n} \rightarrow p + e^- + \bar{\nu}_e \tag{2.5}$$

This reaction releases 782 keV of energy that is distributed among the decay particles.

Neutrons typically have a nuclear binding energy in the MeV scale (around 5 to 9 MeV for materials with atomic mass number A $\geq$ 3). Concerning this work, the weak force does not play a significant role in transmission experiments. Flight times through even the longest tubes are in the order of a few seconds, in comparison to the neutron lifetime of $\tau_n = 885.7 \pm 0.8$ seconds ([11]). Using the exponential decay law:

$$\text{N(t)} = \text{N}_0 \cdot e^{-\frac{t}{\tau_n}} \tag{2.6}$$

and assuming a 5 second time-of-flight, the fraction of neutrons left is:

$$\text{N(5s)}/N_0 = e^{-\frac{5}{858.7}} = 0.9943 \tag{2.7}$$

where N(t) is the number of neutrons at time t and τ_n the life time of the free neutron. In 5 seconds, we lose about 0.5 percent of the neutrons due to β-decay. Therefore, in our transmission experiments, such losses are very small. As we are making relative measurements with different lengths and therefore flight times, we would be sensitive to a count rate difference resulting from β-decay, however, that effect is on the sub-percent level. In comparison to other systematic and statistical errors, we, therefore, neglect the decay losses. In the storage experiments, however, the neutron lifetime is an important input to correctly calculate the loss-per-bounce coefficient
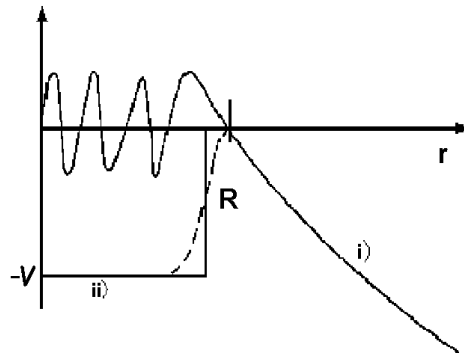
Figure 2.1: A bound state of the neutron. i) neutron wavefunction, ii) neutron potential (dashed line Fermi potential), V is the depth of the potential well inside the nucleus, R the radius of the potential well [10].

μ (see 2.3.2 p.19).

2.1.4   Strong Interaction

A nucleus is a system bound by strong interaction. The force acting between the neutron and a nucleus can be described by a potential well (see Fig. 2.1, p.13). The neutron can either be captured into a bound state in the nucleus (see, e.g., [12], p.243) or be scattered by the nucleus. The strong interaction is one of the channels through which UCN are lost, so any experiment with UCN is affected by the strong interaction.

However, most importantly, the strong force is the interaction, that allows to store UCN. To do that, one sums up the strong force between the neutron and the material surface and thereby obtains the material optical potential.

2.1.5 Material Optical Potential

As pertubation theory can not be applied directly to nucleon scattering, Fermi introduced an equivalent potential, that makes it possible to calculate the small changes in the wavefunction outside the nucleus potential. The potential for the scattering from a single nucleus V_F has the form:

$$V_F = \frac{2\pi\hbar^2 a}{\mu}\delta^{(3)}(\vec{r} - \vec{r_n})$$ (2.8)

where r_n is the position of the nucleus, r the position of the neutron and μ the reduced mass. The scattering length a is a characteristic parameter for each isotope.

When scattering on a group of nuclei, one can define two types of scattering processes, the coherent and the incoherent scattering. Coherent scattering occurs, when the outgoing neutron waves, scattered of different nuclei, interfere with each other. Incoherent scattering occurs if the neutron wave is scattered on a single nucleus, which causes the loss of phase correlation between incoming and outgoing wave.

The description via a potential can be carried forward to the case of scattering from surfaces. If one replaces the δ function in equation 2.8 by the density of scattering centers $n(\vec{r})$ and the scattering length by the bound coherent scattering length a_B, one finds the averaged potential:

$$U(\vec{r}) = \frac{2\pi\hbar^2}{m_n} \cdot n(\vec{r}) \cdot a_B$$ (2.9)

This potential is usually referred to as the material optical potential.

With the help of the material optical potential, we can now depict a scattering process like in basic quantum mechanics, a particle incident on a potential step. The solution to the questions of reflection and transmission

fractions can be found in every quantum mechanics text book. One can see that even for neutrons with a kinetic energy smaller than the height of the potential step, there is a certain penetration depth. During that penetration, the UCN can interact with the nuclei inside the surface and be absorbed or up-scattered inelastically.

Considering the material potential to be complex $U = V - iW$ and using the solution for the reflection coefficient from the text books one obtains

$$R = \frac{E^{1/2} - (E - U)^{1/2}}{E^{1/2} + (E - U)^{1/2}}. \tag{2.10}$$

For the usual case, where $W << V$, one can expand the square roots keeping only first-order terms in W. Thus

$$|R|^2 = 1 - 2\frac{W}{V}(\frac{E}{V - E})^{1/2} \equiv 1 - \mu(E, \theta) \tag{2.11}$$

where μ is the loss per bounce probability for the UCN.

The material optical potential is an important concept as its value is critical for UCN transmission and reflection. The neutron guides should have surfaces that reflect as many neutrons as possible, i.e., surfaces with high material potential. Furthermore, the material optical potential is important for experiments measuring UCN transmission through thin foils, as the neutrons have to overcome the potential barrier of the foil to be transmitted.

The loss per bounce probability is an important parameter in storage experiments. In case of the UCN guides, one needs a low loss per bounce probability to get a high UCN transmission.

2.1.6 Comparison of the Forces

The typical range of kinetic energies for a UCN is 0 - 300 neV. This energy is of similar order of magnitude as the one caused by several other interactions:

- Gravity accounts for a difference of 102 neV per meter in height.

- The material optical potential (strong interaction) of commonly available materials is up to 335 neV.

- A magnetic field of 1.7 T (a magnitude that can easily be obtained for an experiment), accounts for a potential energy of ± 102 neV (see 2.1.2).

It is very rare to find these three forces to be of equal magnitude, as in comparison to strong interaction, the coupling constant of gravity has a relative strength of 10^{-39}, and the one of electromagnetism of 10^{-2} (see [13]).

2.2 UCN Transport and Transmission

2.2.1 Transmissions Experiments

The setup for transmission experiments will be described in chapter 4. The setup must fulfill the following requirements:

- A UCN pulse (from the chopper) enters our guide at a defined point.

- The neutron flux is measured at two different distances from the chopper.

For our analysis, the assumptions are the following:

- The angular and energy distribution of the UCN do not depend on the different distances from the chopper [2].

- The influences of β-decay and gravity are negligible.

With the neutron count rate $J(z)$ at distance z from the source, the transmission probability is:

$$W = \frac{J(z_1)}{J(z_0)} \tag{2.12}$$

The $J(z)$ are measured count rates, see also chapters 4 and 5.

2.2.2 UCN Transport

When UCN propagate along a UCN guide, they can be reflected via specular or diffuse reflection. The fraction of diffusely reflected neutrons is a characterizing parameter of a UCN guide which we want to determine in our transmission measurements.

The model of rarified gas flow can be used to describe UCN transport behavior (see also [10] p.90). In this model, three assumptions are made:

1. The probability for specular reflection is much larger than the one for diffuse reflection.

2. Reflections are mostly elastic scattering processes.

3. UCN can be lost from the system by nuclear absorption or up-scattering[3].

Reference [10] shows two formulae in Chapter 4.4.2 to calculate the transmission probability W through a neutron guide with length Z, radius R and

---

[2]Only valid for experiments carried out with guide lengths not too different.

[3]If a neutron collides with a crystal lattice it can absorb a phonon. The phonon energy will be transformed into kinetic energy of the neutron, which will increase the kinetic energy of the UCN above the level of the material optical potential of the guide and, therefore, the neutron will be lost. Wall scattering also involves elastic scattering with the single nuclei of the lattice, thus if not scattered in the center of mass system, such a scatter process can also increase the kinetic energy of the UCN.

the probability for diffuse reflection f (supposed to be homogeneous over the whole guide surface).

$$W = \frac{2-f}{f} \cdot \frac{8R}{3Z} \qquad\qquad \text{for long tubes} \qquad (2.13)$$

$$W = \left(1 + \frac{3Zf}{8R(2-f)}\right)^{-1} \qquad\qquad \text{for short tubes} \qquad (2.14)$$

With the tubes investigated in this thesis, it is sufficient to use the short tube formula.

Using the second formula introduced above, we can calculate a value for f:

$$f = \frac{2}{\frac{3\ z\ W}{8\ R\ (1-W)} + 1}. \qquad (2.15)$$

2.3   UCN Losses

2.3.1   UCN Loss Channels

If a UCN propagates along its flight path in the experiment there are several processes that can lead to its disappearance:

- Wall losses:

  The wall losses are a combination of different effects. The neutron can be absorbed by the nuclei of the wall material. It can also gain energy in an inelastic scatter process with the wall atoms and, therefore, be lost as the critical velocity might be reached. A UCN can also scatter on lattice phonons and gain energy. This process is referred to as "thermal up-scattering" or just "up-scattering".

- Collisions with atoms of the rest gas:

  All experiments are carried out in vacuum, but there are still some left over atoms. UCN can collide with these atoms and be absorbed

or up-scattered. In our experiment, the vacuum usually is 10^{-4} mbar or better, and this effect is negligible.

- Losses into slits in the setup:

  The experimental setup might have slits that can result from imprecise alignment of the parts or by limits on the accuracy from the machining process. Slits are gaps between neighboring parts of the setup and may be very small, but if a neutron enters a slit it is likely to be lost due to absorption or up-scattering in the slit, because here the bounce rate on the wall gets very high (the mean free path is on the order of the slit width). Losses due to slits are proportional to the fraction of the slit area to the total guide surface.

- β-decay (see Eq. 2.5):

  The β-decay is obviously a limitation which can not be manipulated. However, the other losses are typically far greater, also in all cases studied here.

The relative importance of the different channels may vary from experiment to experiment.

2.3.2 The Loss Coefficient μ

One important loss channel in transmission experiments is wall losses. One defines a loss-per-bounce parameter μ, which gives the probability for a neutron to be lost in one wall collision; μ is characteristic for a specific material and isotope, assuming that the thickness and the quality of the surface are always the same. Finding a value of μ for each guide will be one of the aims of the storage experiments.

2.3.3   Storage Curves and Lifetime

When neutrons are trapped in a storage vessel they can either decay via the weak interaction or be lost (as described above). To calculate the number of neutrons in a trap after a time t, we use equation 2.6, with τ now being the so called storage time constant. Here, τ is a combination of all loss channels, being approximated to be composed of wall losses, losses in slits or holes, and β-decay:

$$\frac{1}{\tau} \; = \; \frac{1}{\tau_n} + \frac{1}{\tau_\mu} + \frac{1}{\tau_{\text{holes}}} \tag{2.16}$$

with:

$$\frac{1}{\tau_\mu} \; = \; \bar{\nu} \cdot \mu. \tag{2.17}$$

Here τ_n is the neutron lifetime, $\bar{\nu}$ the mean wall reflection frequency and μ the loss-per-bounce probability introduced above. The slits and holes in the storage volume are accounted for in τ_{holes}, which is a characteristic parameter for a specific setup.

Using the PDG([11]) value for the neutron lifetime and Monte Carlo simulations to find an average UCN path length for the given UCN energy spectrum, one can derive a value for μ from the measured storage time.

Chapter 3

Hardware

3.1 Neutron Guides

3.1.1 The Glass Tubes

The glass neutron guides begin the production process as borosilicate glass tubes (DURAN©) fabricated by Schott in Germany. The tubes have different lengths, according to their position in the system. The inner diameter is 180 mm and the wall thickness is 5 mm. The reason to make the neutron guides out of glass, despite of all the possible problems this material might have, is that the small roughness of glass is virtually impossible to achieve with common UCN guide materials, such as polished stainless steel. The typical roughness in the glass tubes is less than 5 nm. In steel, a roughness of better than 250 nm after electropolishing is considered to be very good. Surface roughness was found to be a crucial parameter for the characterization of neutron guides, because the probability of diffuse reflection rises with the surface roughness of the guide [14].

3.1.2 End pieces

To be able to connect the neutron guides to the other parts of the guide system, stainless steel flanges are glued to the end of the glass tube. To minimize the slits in the system, the steel flange has to fit very precisely on the glass. To achieve that, we fabricate glass end pieces which are rammed at the end and then machined to fit into the steel flanges. These end pieces are then joined with the glass tube inside a furnace. The steel flanges are then glued to the machined ends.

Figure 3.1: The machined glass end piece joined to a glass tube inside the furnace.

3.1.3 Cleaning

The glass tubes are sealed directly after exiting the furnace. Still the surfaces are heavily contaminated with dust particles. We tried different methods to clean the surface in order to get it as dust free as possible. Dust on the

surface of the tube poses a problem, as every dust particle creates not only additional roughness, but also might create a hole in the coating if it comes off after the coating process. The most promising methods among those employed were i) acid edging in a professional tube cleaning and edging facility and ii) a multi step cleaning process by hand.

In the professional facility, the tubes were first rinsed with deionized water, then bathed in a 5% hydrofluoric acid solution, and finally rinsed 10 times with deionized water.

The manual washing process consists of high speed scrubbing the surface with sponges and soap water, rinsing the tube with hot water, and then with demineralized water, and finally rinsing the tube with different alcohols of very high purity.

Atomic force microscope measurements have shown that the increase in roughness that arises from the acid edging is a factor of 6 and worsens the transmission by roughly 10%. Therefore, the UCN guides will be cleaned by the described manual process.

3.1.4 Coating

The guides are coated once the flanges are glued to the ends and the guide has been cleaned. Then NiMo (nickel-molybdenum) with a weight ratio of 85/15 is sputtered on the surface by S-DH GmbH[1]. The coating was selected to be 500 nm thick. This is enough to act as a barrier for the neutrons and a good compromise in terms of roughness, as the roughness increases with the film thickness. However, the coating also covers some remaining micro dust particles. To keep the surface as dust-free as possible, the tubes are sealed with an especially developed tool and only re-opened inside the sputtering

---

[1]S-DH GmbH, Sputter-Dünnschichttechnik, Hans-Bunte-Strasse 8-10, 69123 Heidelberg, Germany, `www.s-dh.de`

facility once the vacuum is below 10^{-1} mbar.

3.1.5 Placement of the Guides

Figure 3.3 shows the placement of the UCN guides within the PSI UCN source. There are two guides situated at the bottom of the storage volume, extracting UCN of the full available energy spectrum. There is also one guide on top of the storage volume, which can only extract very slow UCN. This guide will mainly be used for R&D purposes.

The glass tubes are not connected directly to the storage volume but to a so called thermo-adapter. This is a stainless steel part used to avoid too much thermal stress on the glass coming from the temperature difference between the storage volume (60 K) and the glass tubes (room temperature). The first meter of guide has to provide thermal adaptation between these two temperatures. Furthermore, the glass would suffer from radiation damage if it was placed so close to the source.

At the end of the thermo-adapter, where it connects to the UCN storage volume, there are remotely controlled flaps, which can open or close the UCN guide. To provide a maximum number of UCN to an experiment, one reduces the volume between source and experiment by closing other UCN guides.

There is a second stainless steel part in each guide, a 30 degree bend, to avoid direct sight of the storage volume. This reduces the neutron and γ background in the experimental area. This bend can not be manufactured from glass of 180mm diameter with reliable precision at reasonable costs and thus was made of steel. All steel parts will also be coated with NiMo, here the dust is less of an issue as the V_F of steel is close to that of NiMo, meaning that a hole in the coating would not lead to significant losses.

(a) Uncoated guide with flanges glued on the ends.
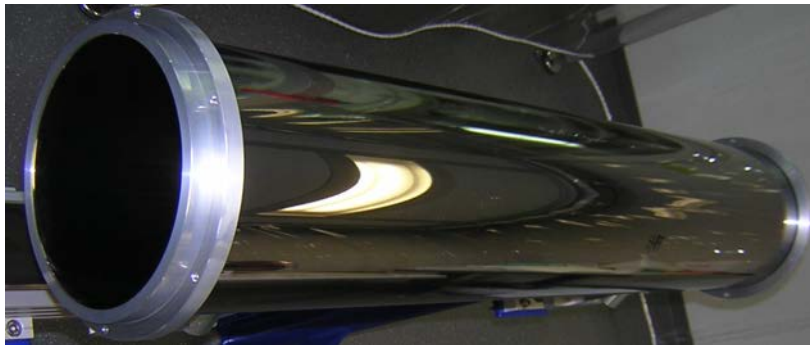
(b) Coated guide, ready for storage and transmission measurements.
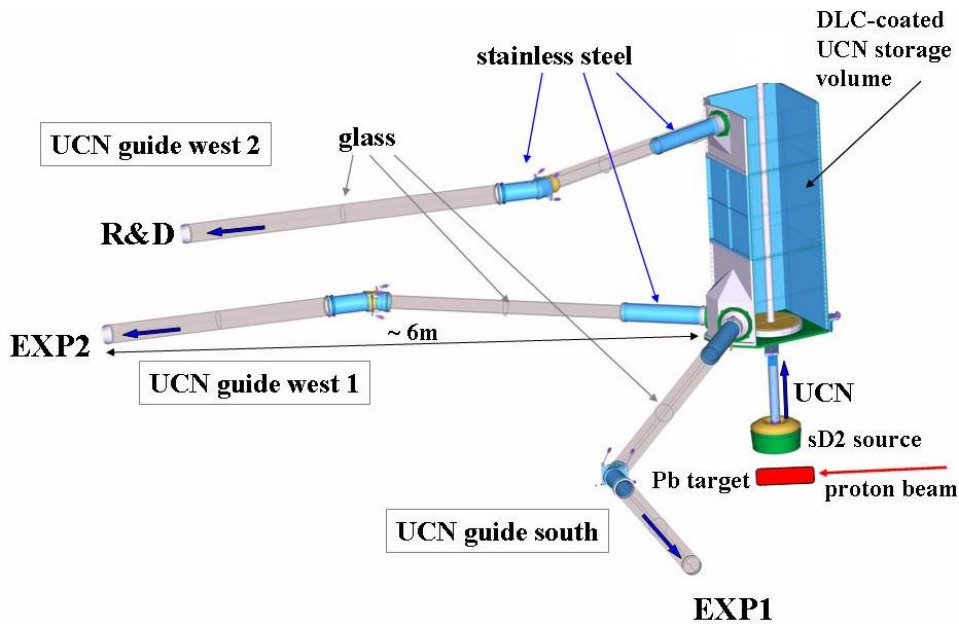
Figure 3.2: Glass tube before and after coating.

Figure 3.3: Sketch of the UCN storage volume and the connected UCN guides, leading to the two experiment areas.

3.2 Vacuum and Neutron Shutters

In the PSI UCN source, the neutron guide system will include custom designed VAT shutters[2] that can be used to separate installed experiments from the UCN source not only in terms of vacuum but also in terms of neutron flux. They are placed at the end of the neutron guides so that they can close the guide towards the source. These shutters consist of a body made of aluminum and a DLC coated shutter disc inside the body, that can be moved either into the beam or out of the beam. The shutter is drawn in Fig. 3.4, p.27. When the disc is retracted, the slit that results from the missing disc at the center of the shutter, is covered by a expanding ring also coated with DLC, attached to the lower end of the disc. This is done because the

---

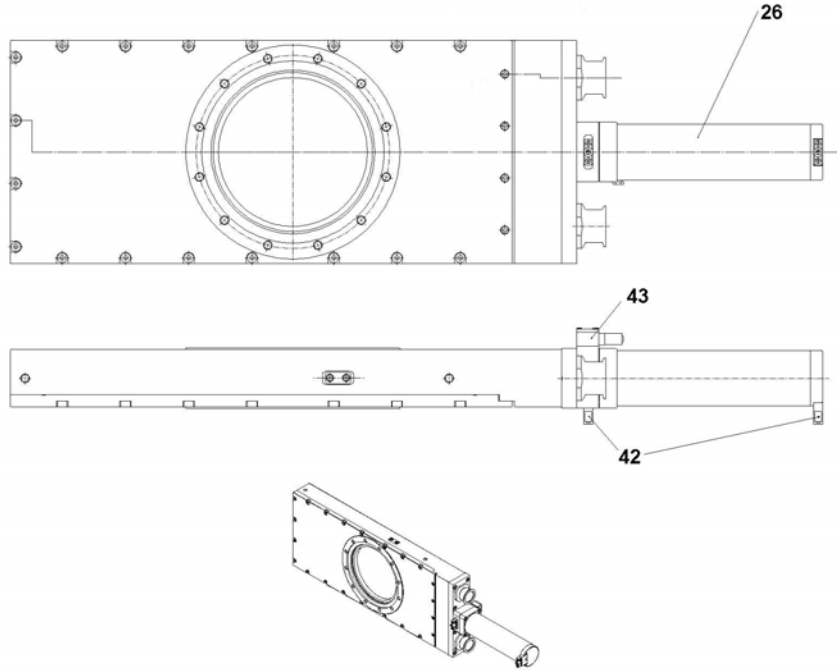[2]VAT Vakuumventile AG, Seelistrasse, 9469 Haag, Schweiz, www.vat.ch

Figure 3.4: Engineering drawing of the VAT shutter. The ring in the middle is the flange, that will be connected to the neutron guide. 26: double-acting cylinder responsible for the shutter movement. 42: end position switch. 43: steering shutter that controls the air flow.

slit has a width of more than 25mm. An open slit of that size would cause relevant UCN losses. The VAT shutter and the moving parts are shown in Fig. 3.5 p.28. The shutter discs are moved with compressed air, which in turn is controlled with electric valves. The typical moving time is about 2 seconds. The discs are coated with DLC and therefore act as UCN mirrors when placed in the beam. Furthermore, because of this coating, the spectrum of UCN that can be stored, extends to higher energies. If a storage volume would have uncoated vacuum shutters as end caps, the losses due to transmission through the stainless steel disc would be higher than with the DLC coating. Before the guides and the shutters will be finally mounted,

(a) Shutter disc (right) and expanding rings for slit reduction in the open position (left).

(b) VAT shutter in action, the outer metal ring with the holes around it will be flanged to the neutron guide vacuum tubes.

Figure 3.5: Working principle of the VAT shutters.

the VAT shutters will be used as shutters in experiments to test the UCN guides.

An electric valve, mounted on the shutter, controls, which of the two inputs of a double-acting cylinder[3], moving the inner parts of the shutter, is connected to the compressed air. The electric control valve consists of a movable channel for the compressed air and a coil which can switch between different channels depending on the current flowing through it. When the current is low, a mechanical spring keeps the channel in default position. The control valve opens the shutter, when connected to 24V and closes the shutter actively, when the voltage is low. This configuration is a safety feature, as in case of a power failure the shutters should close right after the failure. Another important detail is, that the cylinder has an intrinsic

---

[3]A double-acting cylinder is a pneumatic actuator, that can direct its energy in two directions, i.e., it gives the possibility to actively move a device in two directions just with compressed air, as opposed to a single-acting cylinder, which can only be moved in one direction and then has to be moved back by an outer force.

brake, which acts, when the disc reaches one of the two end positions. This prevents damage of the disc or other moving parts.

3.3 Shutter Control Box

To control the VAT shutters, in principle, a 24 V power supply would be sufficient. However, in the process of this work, a control box was built, that allows not only to control a total of 4 shutters, but also to do this either manually, by pushing buttons, or remotely, via software. Furthermore, the box allows monitoring of the shutter disc positions. The next section describes the details of the box and the connection to the VAT shutters.

3.3.1 Modular Electronics Rack

Figure 3.6: The control box, components from left to right: the power switch with the mounted 5 V power supply, the 24 V power supply, the master board, the slave board and finally the National Instruments board.

The control box (shown in Fig. 3.6 p. 29) consists of several modules in an ELMA 19" electronics rack[4]. Individual units can be inserted or removed from the front of the electronics rack. These units consist of a front panel, which is attached to a so called Eurocard, a printed circuit board (PCB) with a 64 pin connector at the end. This connector has a counter part in the ELMA rack, to connect the unit to the power supplies or to signal lines. The modular approach allows for easy testing and shorter repair times.

3.3.2 Power Supplies

The system contains two power supplies. There is one power supply that provides 5 V up to 6.0 A (Astrodyne[5], MSCA-0301) and one that provides 24 V up to 2.0 A (Kniel[6]: 101-018-02 Type: C24.2). The 5 V power supply is mounted onto a power-switch board responsible for the whole box. The 24 V supplies the individual LOGO! components (see below).

3.3.3 Logic Modules

As mentioned above, the shutters can be operated manually or via a computer. To make that possible, there are two Siemens LOGO! 24RCo [15] modules in the box. These modules have 8 digital input channels and 4 outputs. Furthermore, they have an on-board memory that is used to save "programs". These programs specify the output level (0 V or 24 V) for every individual output as a function of the inputs. They also allow for some basic logic functions like AND, OR, XOR etc. for comparisons between different inputs.

---

[4]Elma Electronic AG, Hofstrasse 93, CH-8620, Wetzikon, `http://www.elma.com/Switzerland/English/Products.aspx`

[5]Astrodyne Europe Sales Office 19F, NO. 77, Sec 1 Hsin Tai Wu Rd. Hsi Chih, Taipei Hsien Taiwan, R.O.C., `www.Astrodyne.com`

[6]Kniel System-Electronic GmbH Kurzheckweg 8, Karlsruhe, D-76187, `www.kniel.de`

What was called outputs earlier are switches in the modules, that are opened or closed by the LOGO! program. In this application, one side of the switch is connected to the +24 V power supply, the other is connected to the shutter, which makes the shutter side of the switch a quasi-output. The LOGO! modules process the switching of buttons and are controlled via a NI6501 USB card from National Instruments[7] (NI card) which is explained in more detail in section 3.3.4. The detailed schematics and a visualization of the programm on the LOGO! modules can be found in appendix B (p. i).

Two LOGO! modules mounted on two boards in the box control two shutters each. There is one master board and one slave board. The main difference between these units is that the button to choose the operational mode (manual or computer) is mounted on the master board. This status is conveyed to the slave board through a cable in the back of the box. Furthermore, the master board uses two outputs of the Siemens LOGO! module to indicate the modus operandi.

Figure 3.7 (p.32) shows the master board with three buttons on the front panel, the top one selects between manual mode and computer mode, the two lower ones are altering the shutter position of one shutter each.

The slave board seen in Fig. 3.8 (p.33) has only two buttons, one for each shutter. Both boards have LEDs next to the buttons, the red and green LEDs indicate the position of the shutter discs; red indicates a closed, green an open shutter. Should no LED be illuminated, then the shutter is in motion (or a LED is broken). The LEDs are connected to the 5 V power supply via switches in the shutter frame. These switches are closed when the shutter discs reach an end position. The position information is then again conveyed to the NI-board. On the master board, next to the switch

---

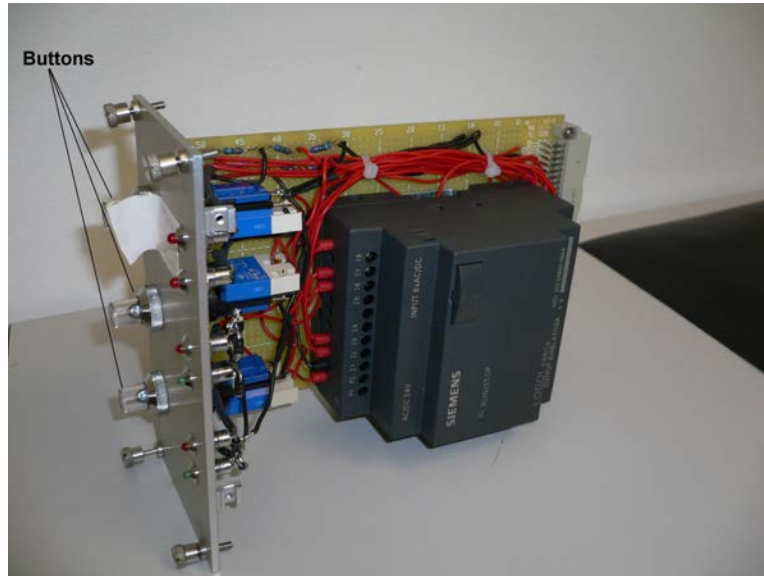[7]National Instruments Switzerland Sonnenbergstr. 53 CH-5408 Ennetbaden, `www.ni.com/de/`

Figure 3.7: The master board.

choosing the modus operandi, there are two red LEDs indicating, wether the manual controls or the computer controls are active. This signal, too, is forwarded to the NI card.

3.3.4 Digital I/O

A digital I/O card is used to communicate between computer and the LOGO! modules via TTL[8] signals. A NI USB 6501 card was chosen because it is cheap and it works via USB, which simplifies the connectivity. Mounted on the NI-board are the NI-card, but also an Infineon-semiconductor chip (part number: ITS711L1), to transform 5 V signals into 24 V signals. The position signal from the shutter disc is directly fed into the card as well as the signal about the modus operandi. The outputs that are used to move

---

[8]TTL stands for Transistor Transistor Logic and in this case means a 5 V binary logic system: +5 V corresponds to the logical state 1, 0 V to the state 0, there are other TTL standards, but this is the most common for this type of application
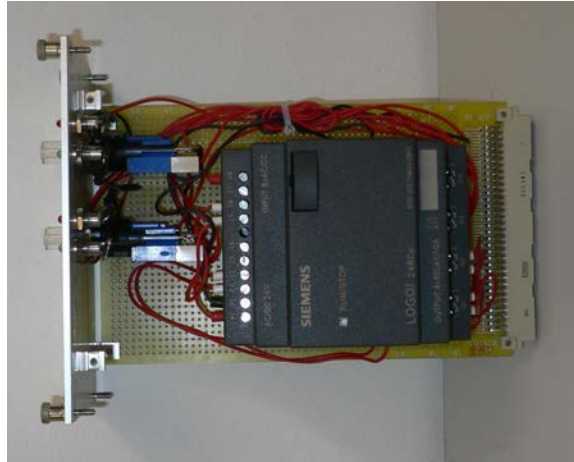
Figure 3.8: The slave board. Only two buttons are on the front panel. No output of the LOGO! is used to indicate the modus operandi, i.e., there are two outputs left on this board.

the shutters, are transformed to 24 V logic and then sent to the LOGO! modules.

One of the advantages of using a National Instruments card is, that all NI-components are compatible with LabView, a programming language by National Instruments for data acquisition and control of peripheral components, i.e., the NI card. A LabView program allows the user to see the status of the shutter and the modus operandi of the box on his screen (virtual LEDs), and a remote control of the shutter.

3.3.5 Operating Voltage

All control signals are 24 V pulses[9] generated either by connecting the 24 V power supply to the input of a LOGO! module via a normally open[10] switch,

---

[9]The exact shape or length of the pulse is irrelevant, the LOGO! module reacts to the rising slope of the signal.

[10]Normally open means that the switch is open as long as it is not pressed, while pressed the current flows through the switch and the switch is reopened as soon as the button is released.

or by transforming the TTL signals from the NI card to a 24 V signal. This configuration was dictated by the fact, that not only the electric valves mounted on the shutters but also the Siemens LOGO!- modules are only available with 24 V DC operational voltage. A digital I/O card with 24 V logic however would have been more expensive by an order of magnitude.

3.3.6 Connection between Box and Shutter

Every shutter has been set up with a cable that can be connected to the box via a round 8-pin Burndy plug. Figure 3.9 (p. 34) shows the plug for the cable mounted to the box. The middle pin is the ground line, used for the
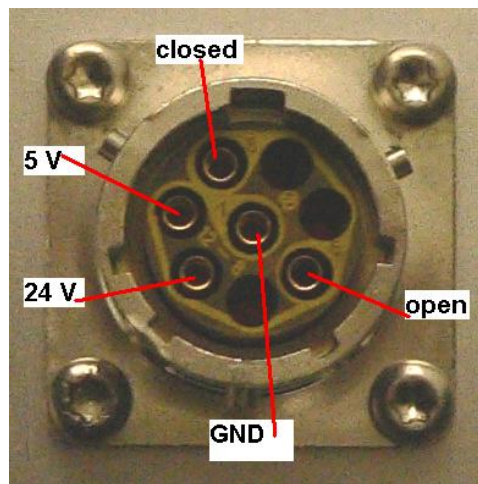

Figure 3.9: The 8-pin plug of which only 5 pins are in use. The pins with the title "open" and "closed" carry 5 V, whenever one of the end switches for those two positions is closed.

shutter coil and as low signal for the NI-card. Pin 2 carries 5 V for the two end position switches. These switches are closed by the piston that moves the shutter disc. When the shutter is completely closed, the end switch for the closed position in the shutter body is closed and the 5 V from pin 2 are

connected to the box via pin 8. The same is true for the final position open. Only then the 5 V are on pin 5. Pin 3 carries 24 V whenever the shutter is meant to be open, i.e., when the LOGO! returns 24 V.

3.3.7   Brief summary

The power comes from two power supplies in the box, one 5 V and one 24 V supply. There are two possibilities to alter the shutter state, manually or with a computer. Both inputs are fed into the LOGO! module, which acts as a switch for the 24 V towards the shutter. If a shutter reaches one of the two end positions, it closes an end position switch, which conveys a signal to LEDs on the box and to a computer, if connected. There is one button on the box that allows to choose between the two inputs, computer or manual. It is an XOR situation, i.e., only one of the two controls works at a time and the computer user can not change the input channel. Compared to a standard Windows computer, that would make the manual user the system administrator and the computer user a guest. This was implemented with regard to the foreseen experimental situation. Once the system is installed, there might be some situations where it is in the interest of the source team to close the shutters to the experiments and to make it impossible for the guest scientists to reopen them. However, if necessary one could enable the computer to change the state of the box by soldering one more wire into the box and by slightly altering the program on the LOGO! modules.
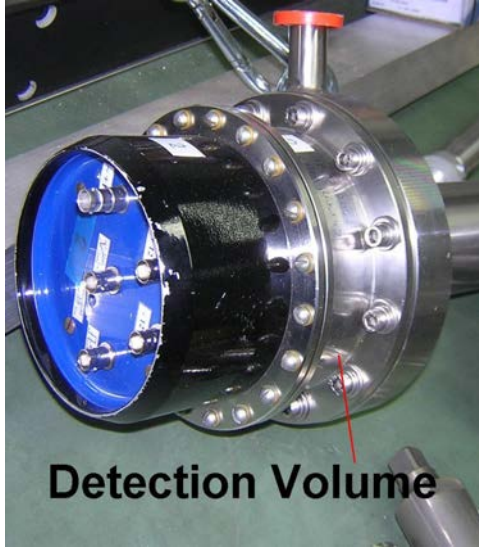
Figure 3.10: ^{3}He counter

3.4 ^{3}He Counter

In our experiments, we use two different types of UCN detectors, a ^{3}He counter and a fast GEM based detector. The ^{3}He counter, see Fig. 3.10, was purchased from the Frank Laboratory of Neutron Physics at the Joint Institute for Nuclear Research, JINR, in Dubna. Neutrons are detected in the gas detector volume after passing through a 100 μm aluminium window. The gas is a mixture of ^{3}He at 18 mbar, CO_2 at 10 mbar and as much argon as needed to make a total pressure in the detector volume of 1.1 bar. When a neutron is captured by a ^{3}He nucleus, the following nuclear reaction occurs:

$$^3He \; + \; n \; \longrightarrow \; ^3H \; + \; p \; + 0.764 \text{ MeV} \qquad (3.1)$$
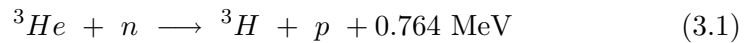
Due to the high neutron capture cross-section of ^{3}He, only little amounts of the gas are needed to obtain a high detection efficiency for UCN.

There is a gold plated tungsten wire under high voltage in the middle of the detector. This wire attracts and gas amplifies the electrons that are produced when the proton or the triton ionize argon atoms. The resulting charge pulse in the wire can be measured. The proton and the triton can also excite argon atoms without ionizing them. Then, these emit UV photons which could cause a continuous discharge in the detector. To overcome this problem, CO_2 is added as a so called quenching gas. The CO_2 absorbs the photons and prevents further discharge.

The advantage of the ^{3}He counter is its very high detection efficiency (close to 100%). The detector efficiency cancels out in the analysis, so it is not vital to know it to a high precision for our purposes.

The disadvantage of the ^{3}He counter is that it has no spatial resolution and an entrance window with a diameter much smaller than that of the UCN guides we want to characterize. Some improvement is achieved by changing to the Cascade-U detector (see Sec.3.6, p.39).

The ^{3}He counters used in our experiments were all connected to a high voltage of 1 kV and the signal was pre-amplified in the detector to a negative pulse of up to 100 mV. This negative pulse was then fed into the data acquisition system (DAQ), see below.

3.5   Data Acquisition System for the ^{3}He Counters

The ^{3}He counter DAQ consist of several different NIM modules and a Fast ComTec [11] Multi-Input Multi Channel Analyzer System (MPA-3). Following the scheme shown in Fig. 3.11, the signal from the detector is fed into a spectroscopy amplifier, the unipolar signal output from the amplifier is split and fed into i) a delay amplifier and ii) a discriminator (SCA). If the discrim-
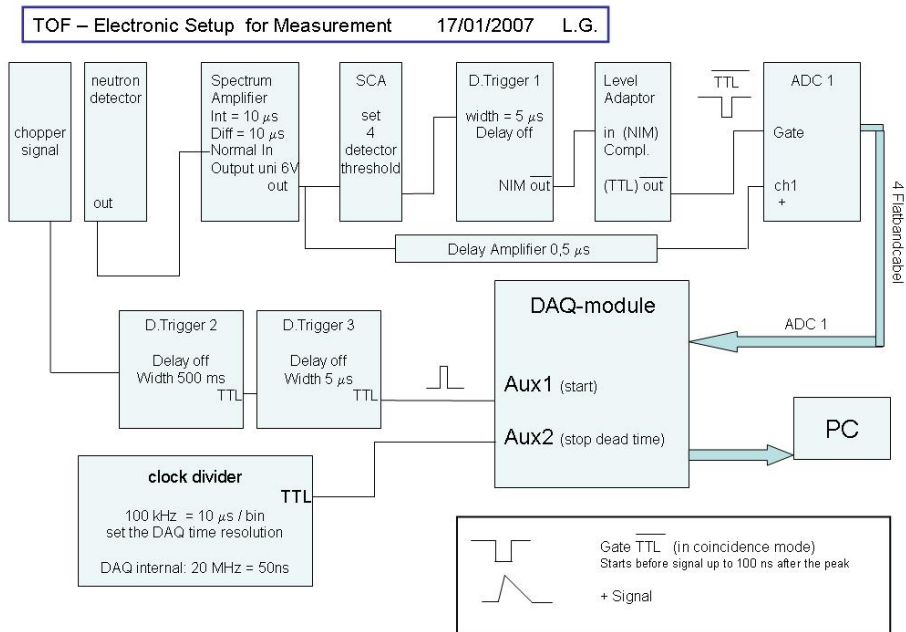
―――――――――
[11]http://www.fastcomtec.com/

Figure 3.11: Schematic of the ^{3}He detector signal processing up to the DAQ

inator identifies the signal as valid, it creates a TTL that passes through a delay trigger and a signal converter. The output of the signal converter is an inverted TTL signal which acts as a gate for the ADC. The delay amplifier compensates the delay in the discriminator, the delay trigger and the signal converter needed for the signal processing. With correct settings, the signal should then produce its own gate.
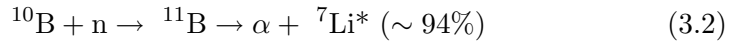
The schematics for TOF-measurements is shown in Fig. 3.11 (p.38) (The setup for the monitor detector is not shown here).

The delay triggers inserted between the chopper and the DAQ system are used to shape the chopper signal to a proper TTL signal, needed to avoid ambiguities.
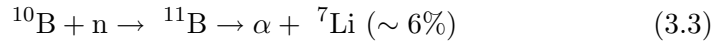
3.6 Cascade-U Detector

Cascade-U[12] stands for Cascade detector for ultra-cold neutrons. It is a neutron detector using a ^{10}B solid state converter. The detector is customized for the use with UCN.

The detection of neutrons goes via nuclear caption in a boron layer, vapor deposited on the 100 μm detector entrance foil made of aluminium. The neutron triggers one of the following two nuclear reactions:

$$^{10}\text{B} + \text{n} \rightarrow\ ^{11}\text{B} \rightarrow \alpha +\ ^{7}\text{Li* } (\sim 94\%) \tag{3.2}$$

or

$$^{10}\text{B} + \text{n} \rightarrow\ ^{11}\text{B} \rightarrow \alpha +\ ^{7}\text{Li } (\sim 6\%) \tag{3.3}$$

The α and the ^{7}Li have kinetic energies of 1.47 MeV and 0.84 MeV, respectively, and leave ionization tracks while moving through counting gas (argon) in the detector volume. The ionization leaves free electrons, which are amplified through a GEM[13] foil (see Fig. 22). The electrons are gas amplified by the potential difference between the two copper layers of the GEM. As in the ^{3}He counter, there is CO_2 in the detector, acting as quenching gas. The electron clouds from the GEM can then be detected with a 2D spacial resolution of 1 to 5 mm depending on the configuration. This is done on a 256 pixel read-out structure, where each pixel has an area of 12.5 x 12.5 mm^2. The 2D spacial resolution allows for more precise analysis (more details will be given in 4.3.11, p.73).

---

[12]for more details on the Cascade-U see `http://www.n-cascade.com/`

[13]GEMs are made from Kapton foils (50-100 μm thick), that are coated on both sides by a thin layer of copper (5-15 μm thick). Most importantly, these foils are covered with a regular pattern of through going holes, 50 μm in diameter and at a lattice spacing of about 150 μm. GEMs were developed by CERN, see `http://cern.ch/gem`
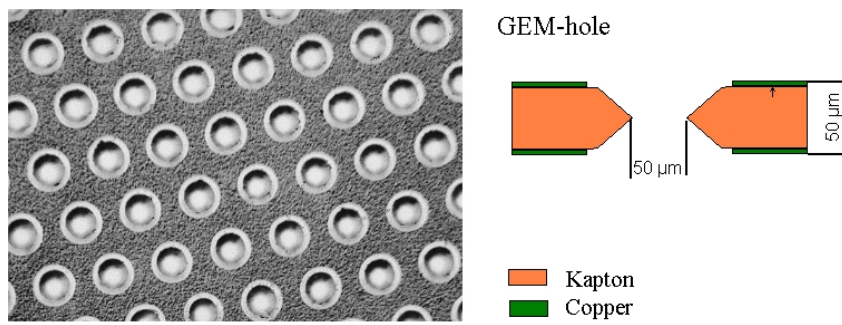
GEM-hole

Kapton
Copper

Figure 3.12: A GEM (Gas Electron Multiplier) foil made of Kapton, coated with copper [16].

UCN

Boron coated
entrance window

GEM

Pixel read-out
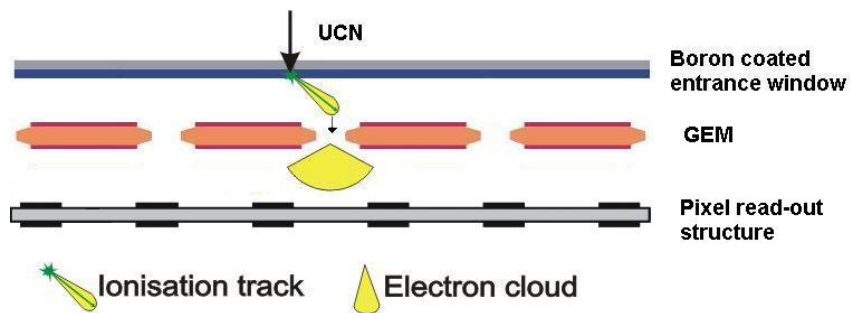structure

Ionisation track   Electron cloud

Figure 3.13: Schematic of the Cascade-U detection principle [16].

The detector is constantly flushed with a gas mixture of argon and CO_2 (with a ratio of 82/18) as a quenching gas. By flushing constantly with new gas, aging effects are minimized.

The Cascade-U detector has several advantages over the ^{3}He counter:

- The Cascade-U is a fast detector, its internal clock runs at 10 MHz. This allows for a high time resolution and therefore high counting rates.

- It has a large detection area of 200 x 200 mm^2 as opposed to a 70 mm diameter circle of the ^{3}He counter. Our neutron guides have a diameter of 180 mm. Measuring them with a ^{3}He counter would mean a loss of more than half of the transmitted neutrons on the reduction flange.

- The solid state converter allows for precise knowledge of the conversion point. This reduces the error on the length of the flight path. In the ^{3}He counter, the neutron is converted in a gas volume of $\sim$6 cm length, in the Cascade-U the uncertainty is limited to the thickness of the boron layer, $\sim$300 nm.

- Disadvantages of the Cascade-U detector are its more complex electronics, the fact that the detector needs a steady gas supply and its larger size and weight.

3.7 Neutron Chopper

One possibility to do transmission experiments is to use a neutron chopper. The chopper provides a pulsed UCN beam from a continuous UCN source

(a) Front view of the neutron chopper, the top cover is taken off, so one can see the axes of the plexiglass discs. Picture (b) shows a zoom into the beam line (red square)

(b) The beam line partially covered by plexiglass discs, the very bottom of the beam is open, the upper part is covered.

by periodically opening and closing the beam line.

Our chopper consists of three counter-rotating plexi-glass discs - each on its own axis - on which the incoming neutron flux is either reflected, up-scattered, or absorbed in the disc and therefore lost. The three discs each have slits. When the slits coincide in the beam line, they open the beam line. The shape is described by the opening function. The opening function is nearly rectangular (see Fig. 4.14 p.67 for the measured shape) and lasts for $\sim$5% of the revolution time. This opening function defines the UCN transmission of the chopper. In our test experiments, the chopper was running at constant frequencies between 0.6 Hz and 1 Hz. This setup is placed in an aluminum container in order to work in the vacuum of the UCN

beam line. The aluminum container has flanges to connect common 70 mm diameter UCN guides on both ends. The chopper was built at PSI by the UCN group, namely Andreas Knecht and Michael Meier (for a description of the principle, see also [17]).

3.7.1 Chopper Characterization

The chopper provides a defined start signal for the TOF measurement via a TTL signal. This signal is created by a photodiode which is shaded by a metal part, mounted on the axis of one revolving disc, at every opening. There is a defined time difference between the TTL signal and the actual opening of the chopper which in the following will be called δt.

UCN velocities are calculated from the TOF - determined from the timing of the chopper signal and the detector signal - and the flight path length. The accuracy of the velocity is therefore directly linked to the accuracy of the chopper timing. The time offset δt has a very large impact on the integral counts in a predefined exact velocity interval, as δt is of the same order of magnitude as the typical TOF. So an uncertainty in the δt value translates into an uncertainty of the calculated velocity. This uncertainty in the velocity leads to an uncertainty in the integral boundaries and in turn to different values for the transmission. The corresponding uncertainty depends on the steepness of the TOF spectrum. Therefore, dedicated measurements of δt were performed. The evaluation of δt and the error resulting from the uncertainty in δt will be explained in chapter 4.3.5 and chapter 4.4.3 respectively.

3.7.2 The Electronic Chopper Signal

Unfortunately, in the present version of the chopper, the opening signal is not a clean TTL signal. The steepness of both slopes of the signal depends on the chopper frequency (this is shown in figure 3.14, p.44), as the signal is generated by a piece of aluminum that is affixed to the axis of one of the three chopper discs. This piece of aluminum shades a photodiode at every rotation. The value of δt depends on the relative placement of this piece of aluminum with respect to the chopper blades.

The shape of the opening signal shown in figures 3.14 and 3.15 shows the shading process. The voltage on the photodiode decreases with decreasing area of the light beam. By using slit collimators, this could be improved. The signal is high when the photodiode is uncovered and low when it is shaded. The electronic chopper signal is a very long signal, as the aluminium
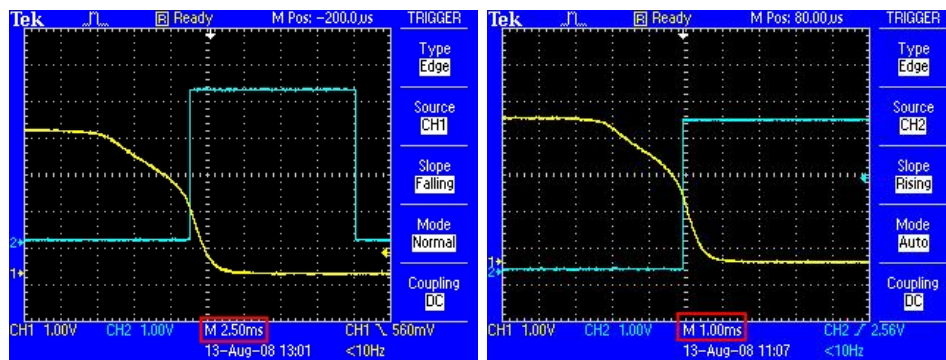

(c) Signal at 0.5 Hz, x-axis: 2.5 ms/unit

(d) Signal at 1.375 Hz, x-axis: 1 ms/unit

Figure 3.14: Chopper signal and its derived TTL signal after shaping. The steepness of the chopper signal changes with the frequency. Note the different x-axis scale.

plate covers the photodiode for almost 6% of the revolution time. This was

measured with an oscilloscope for different chopper frequencies. It triggers the connected delay amplifier when the signal voltage drops to 0, but it also triggers it when rising back to 5 V. This is due to the lack of signal shaping in the chopper electronics. Therefore, we used two delay triggers built at PSI to shape the signal. The first trigger produces a well shaped TTL signal longer than the signal produced by the chopper. The second delay trigger reduces that signal to a short ($\sim$5 μs) pulse to minimize DAQ dead time. Figure 3.15 shows the two TTL signals, at the beginning and at the end of the chopper signal.
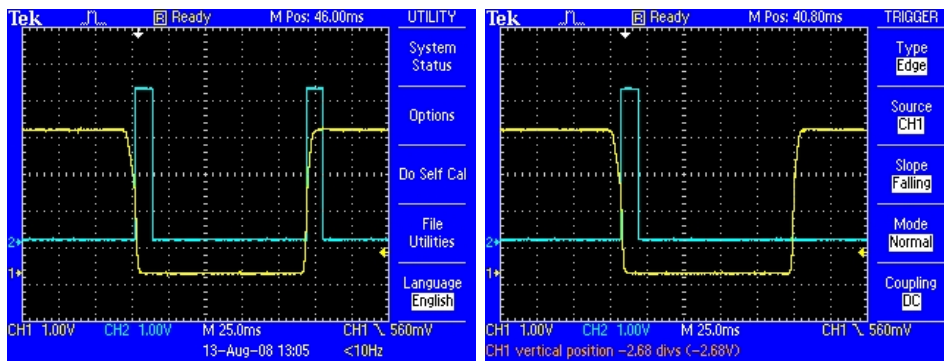
(a) Two trigger pulses, setup with the chopper signal as input of just one delay trigger set to a pulse width of $\sim$18 ms

(b) The same input signal, using two PSI delay triggers for pulse shaping before the DAQ. Only one trigger pulse is left.

Figure 3.15: Chopper signal observed on the Oscilloscope. The yellow line is the direct chopper signal, the blue line the signal after the delay trigger(s).

Figure 3.16: Shielding for the Cascade-U detector. The front parts are placed on top of the box.

3.8 Shielding

The shielding is a vital part of the experimental setup, as in a reactor hall, the background without shielding might be too high to even distinguish the signal from the background. Boron plastic or PE is used to shield the detectors in our setups.

Chapter 4

Transmission Measurements using the TOF Method

4.1 Measurement Principle

Our method of measuring the UCN transmission of a UCN guide is to compare count rates using a defined setup with and without a test guide. The measurements are done using the time-of-flight (TOF) method, see 4.1.1. This allows for an analysis depending on the kinetic energy of the UCN. Figure 4.1 shows a scheme of the setup:
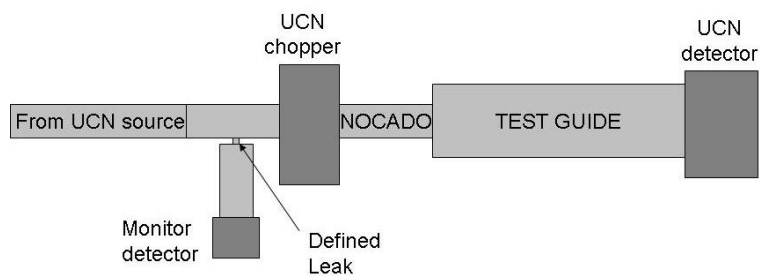

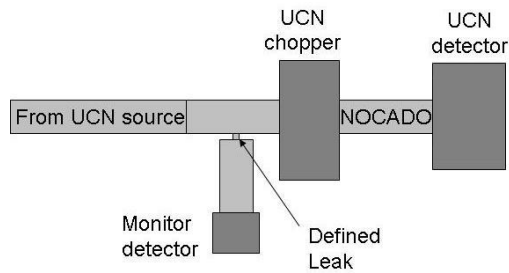Figure 4.1: Scheme for an experimental setup for transmission measurements using the TOF method.

Figure 4.2: Scheme for an experimental setup without the test guide.

The UCN enter the experiment from the UCN source (on the left of the scheme) through a standard UCN guide (a stainless steel tube, with a roughness smaller than 250 nm, produced by the company Nocado[1]). In front of the chopper, some of the UCN are detected in a monitor counter for normalization (see 4.1.2). Behind the chopper, the now pulsed beam passes through a standard Nocado tube, before entering the test guide. At the end of the test guide, the UCN are detected as a function of time (see 4.1.1).

The second measurement for the normalization of the UCN transmission of this test guide is done using the same setup without the test guide (see Fig 4.2, p.48).

---

[1]Nocado GmbH & Co. KG, Kirchweg 3, 26629 Groefehn, Deutschland, `www.nocado.de`.

4.1.1 Time-of-Flight

The time-of-flight (TOF) is recorded in a spectrum started by the electronic chopper signal. With every chopper signal the clock is reset.

It is trivial to calculate the z-component of the UCN velocity (v_z) using the length of the setup L and the TOF:

$$v_z \; = \; \frac{\mathrm{L}}{TOF}.\tag{4.1}$$

A drawback of this technique is that one can only measure the velocity component along the axis of the setup (v_z) and not the absolute velocity. The neutron detectors do not provide information on the kinetic energy.

4.1.2 Monitoring Transmission Experiments

A ^{3}He counter, installed in front of the chopper (see Figs. 4.1 and 4.2) is used to monitor the incoming neutron flux. This is done to observe possible fluctuations in the source intensity, and hence one is able to correct for it.

The monitor detector is installed underneath the beam line which has a small but defined leak that is connected to the detector via standard neutron guides. Placing the detector underneath the beam increases the kinetic energy of the UCN, as to transmit also UCN with $v < 3.3$ m·s^{-1} through the detector entrance window. The size of the leak is small enough not to affect the main neutron beam but large enough to have a reasonable amount of statistics in the monitor counter. The monitoring ^{3}He counter is processed by the DAQ described in chapter 3.5.

Figure 4.3: Setup for the transmission experiment made in Mainz, April 2008.

4.2 Lab Situation

The measurements were done on channel C of the TRIGA facility in Mainz (Germany) and on the UCN test-beam line at ILL. The setup used in both facilities was similar to those sketched in Fig. 4.1 and 4.2.

At ILL, we measured at the test beam of the PF2 instrument on beam height, hence we did not alter the UCN velocity spectrum from the turbine.

In Mainz, we raised the setup 0.5 m over the beam exit. The UCN spectrum in Mainz starts at around 4.5 m·s^{-1} because of the material potential of the deuterium crystal. Raising the setup by 0.5m shifts the spectrum down in energy and increases the UCN rate by almost a factor of 2 (for more details see [9]). To be detected, the UCN have to have a v$_z$ component larger than the critical velocity (v$_c$) of the detector entrance window, in our case ~3.3 m·s^{-1} (v$_c$ of aluminium). Raising the UCN by 0.5 m increases their potential energy by an amount that corresponds to the difference in kinetic energy between UCN of 3.3 m·s^{-1} and 4.5 m·s^{-1}. To raise the beam line,
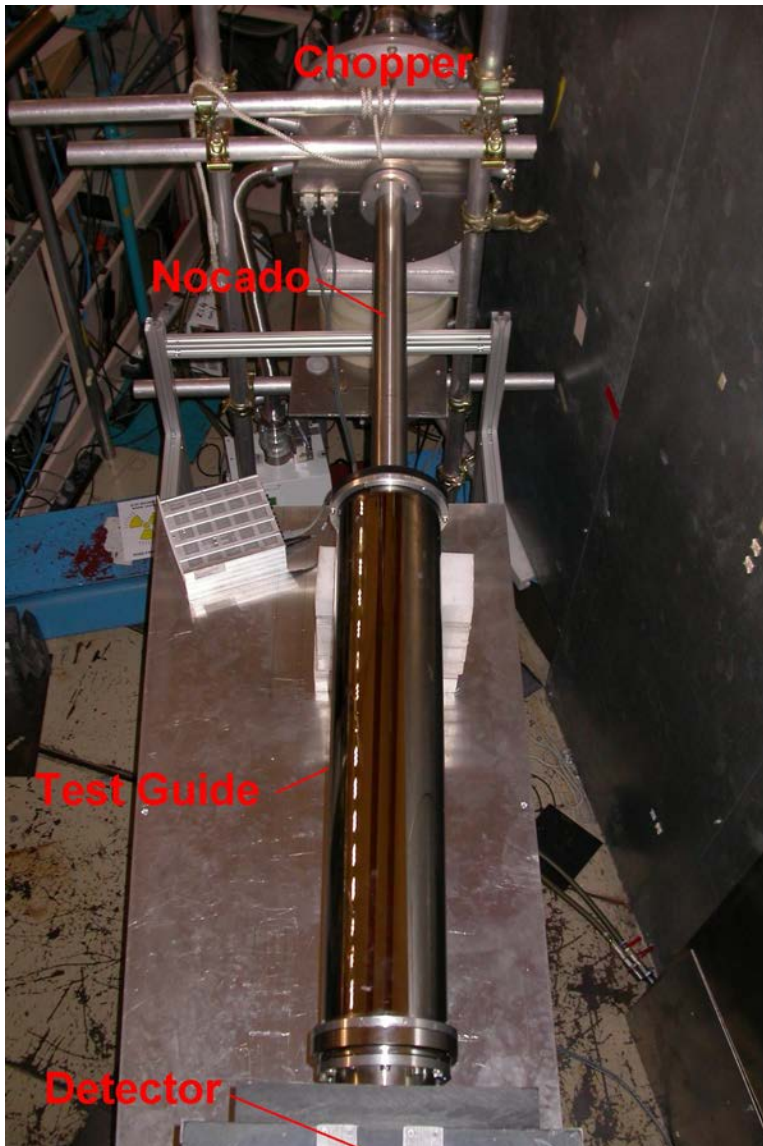
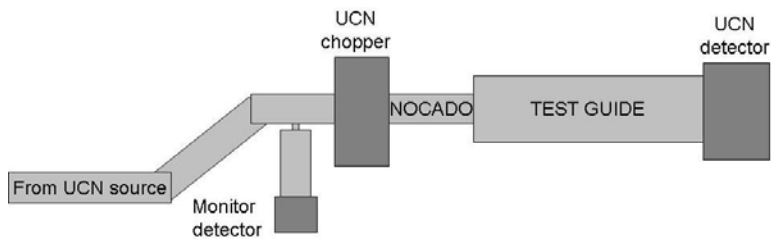Figure 4.4: Transmission experiment made at ILL, July 2008.

Figure 4.5: Experimental setup raised by 0.5 m. (Mainz)

two additional 45° bends were inserted before the chopper, which provided additional cleaning from faster neutrons, see Fig. 4.5.

4.2.1 Vacuum

All experiments were done in vacuum using one pre-vacuum pump and one or two turbo pumps. The usual working vacuum was of the order of 10^{-3}mbar or better. However, at ILL, we have done one measurement with a vacuum of only $3 \cdot 10^{-2}$mbar and the count rate was the same within the error as with a vacuum of $2 \cdot 10^{-3}$mbar.

4.3 Analysis

Several analysis steps are necessary for the determination of a value for the UCN guide transmission:

- Spark removal (see below);

- Background subtraction;

- Normalization to measurement time;

- Correction of the TOF by δt, the chopper time offset;

- Conversion from TOF to a velocity (v_z) spectrum[2];

- Integration of the spectrum over a selected velocity interval.

In the following, I will describe these steps in detail.

4.3.1 Spark Removal

The Cascade-U records TOF spectra, that can have obvious anomalies, i.e., bins with an increased number of counts, called sparks. Figure 4.6 (p.54) shows such a spark. They can result from a short high voltage break-through, i.e., a spark, from the GEM to the read-out structure of the detector. Such a break-through originates from small peaks in the GEM foil surface, e.g. dust particles. Due to the peak shape, the electric field is increased, which in turn increases the magnitude of the ionization charge cloud. With every spark, parts of such a peak are "burnt" away, therefore reducing its size. Consequently, the number of sparks reduces in time. Sparks can also be caused by humidity or impurities in the detector gas.

Spark events deposit a high charge in a few pixels. This charge is then counted as a large number of UCN.[3]

The spark removing part of the analysis works as follows: If a channel of the spectrum is found to exceed the average number of counts of its 30 neighboring channels by more than 5σ, then the bin content is replaced with the mean of the two neighboring channels.

---

[2]This step is only done to visualize the correct velocity spectrum, it is not necessary for the calculation of the UCN transmission.

[3]The Cascade-U was used with two different read-out structures, the first one was sparking very frequently because of its design. The one built in now, has a slightly different design, which reduces the sparking considerably.
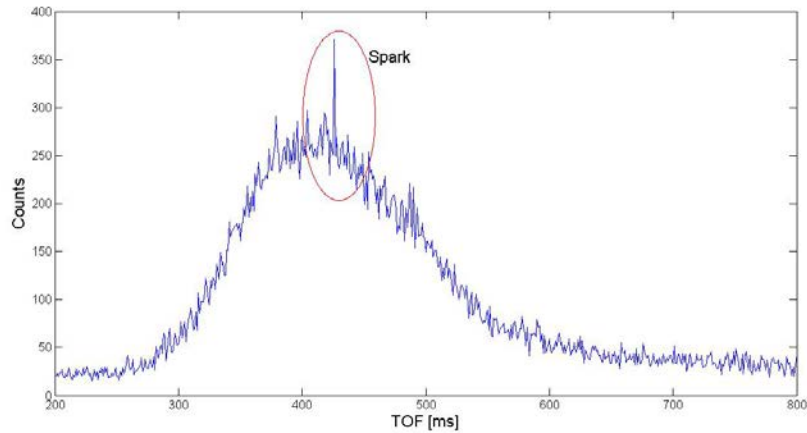
Figure 4.6: TOF spectrum with an anomaly.

4.3.2 Background Subtraction

As all measurements were done in a reactor environment, one expects a considerable background (BG) level. Special measurements with a neutron shutter blocking the UCN source output were performed in order to determine the BG level, i.e., without UCN in the setup. This BG is caused by different sources, the most prominent being the reactor which radiates thermal and fast neutrons. Figure 4.7 (p.55) shows a TOF spectrum with the red line indicating the measured BG level at the detector position. Obviously there is some additional offset in the spectrum.

This offset can be explained as follows: a diffuse reflection of a UCN can alter its axial velocity component, its angle of momentum and even its direction along the guide axis, hence the UCN loses its correlation with the chopper pulse and contributes to a constant BG. The level of this BG is correlated to the length of the guide, as a bigger guide volume also offers a larger storage volume, thus increasing the count rate of stored neutrons
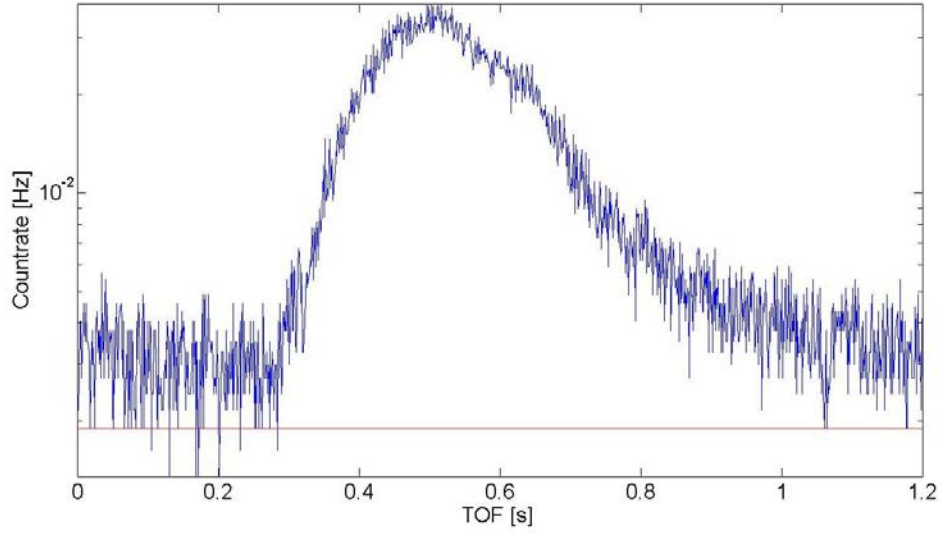
54

Figure 4.7: TOF with BG level indicated by the red line.

reaching the detector. However, we did not determine the exact correlation.

To calculate the transmission of a test guide, we use the following formula (integral boundaries and more detail in chapter 4.3.9):

$$T_g \;=\; \frac{\int \frac{dN_1}{dTOF} dTOF}{\int \frac{dN_2}{dTOF} dTOF}. \tag{4.2}$$

With $\frac{dN_i}{dTOF}$ the count rate for a given TOF interval in a setup 1 (with the test guide) and a setup 2 (without the test guide) (see chapter 4).

If only the measured BG level is subtracted from the measured TOF spectra, the additional offset described above increases the value of the integral with the mounted test guide relative to the case without the test guide. Therefore, the transmission of the guide is artificially increased. To prevent that, the base line of the spectrum is fitted and subtracted as "total BG".
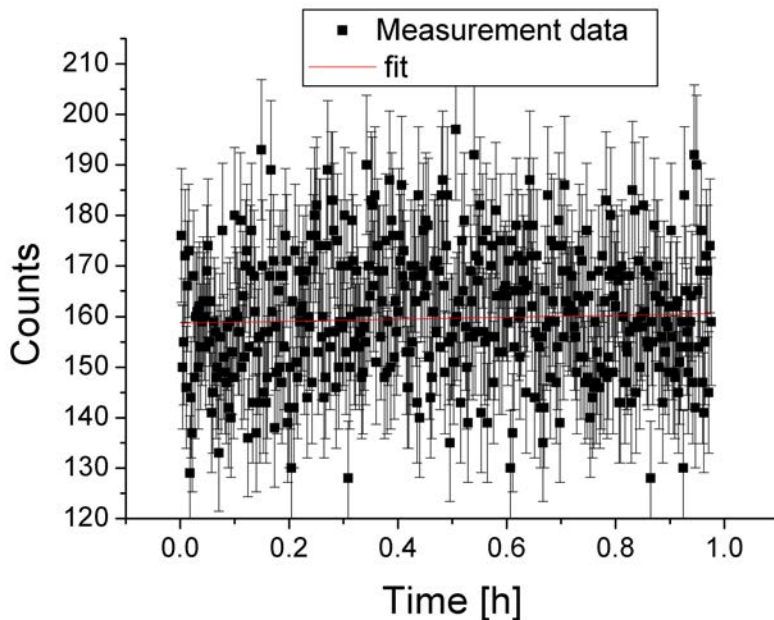
Figure 4.8: Typical monitor counter spectrum at Mainz, plotted over a measurement time of 46 minutes.

4.3.3 Normalization to Measurement Time

The DAQ records a file with the total number of counts in the TOF spectrum, the real time of the measurement, the live time of the DAQ and the number of chopper pulses (sweeps). In order to compare different measurements, one has to normalize the data. We have two means of normalization: i) Normalization to the measurement time or more correct to the live time of the DAQ system. ii) Normalization to the count rate observed in the monitor detector during the measurement. Measurements in Mainz were normalized to the measurement time.

In the following, I will show why the monitor counter was not used for normalization of data taken in Mainz. One reason to use a monitor detector is the possibility to see drifts of the source intensity during i) one measurement and ii) over the course of a day.

56

i) Figure 4.8 (p.56) shows a spectrum recorded with the monitor detector. It was rebinned to 40 s time bins to decrease the uncertainty on the counts per bin. A linear fit of the data gives the following result: $y = 158.7 \pm 1.2 + 0.0006 \pm 0.0006$ with $\frac{\chi^2}{438} = 1.04$. This indicates a purely statistical distribution and suggests that there were no source drifts within this run. The situation is similar for all investigated monitor detector files. As the count rate of the monitor detector is $\sim$2 Hz, and the count rate in the main detector is $\sim$50 Hz, normalizing the measurement data to the monitor detector would enlarge the statistical uncertainty by a factor of $\sqrt[2]{25}$. However, making the leak (see 4.1.2 p.49) towards the monitor counter much larger, and thus increasing statistics in the monitor counter, would strongly influence the measurement.

ii) The distribution of a combination of 5 hours of measurements was also fitted linearly ($y = 399.5 \pm 1.3 - 0.2 \pm 0.4 \cdot x$; the $\frac{\chi}{975}$ was 1.64). This implies the source intensity to be constant over one day of measurements. Figure 4.9 (p.58) shows the counts in the monitor detector over the course of one day (5 h of measurements).

For the measurements performed at ILL, the situation is different.

During our measurements at ILL, the reactor had an unintentional breakdown. We could clearly see the decrease and increase in power as the reactor was ramping power. As an example, Fig 4.10 (p.58) shows a 10% variation in power. This incident was followed by slight reactor power variation (1-3%) during our measurements. Thus, we had to compensate that by normalizing the measured data to the monitor count rate.
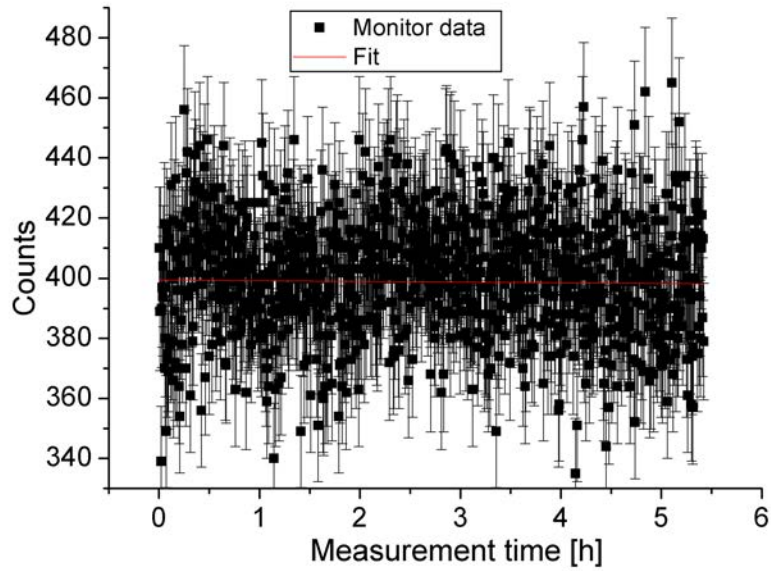
Figure 4.9: Counts per minute in the monitor detector at Mainz. The count rates are statistically distributed, suggesting no drifts or variations of the source intensity.
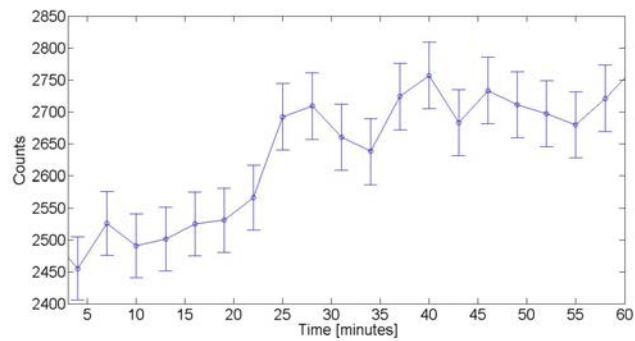

Figure 4.10: Counts in the monitor detector at ILL as a function of time, with the reactor power at ILL rising from ~ 52 to ~ 57 MW in one hour.

4.3.4 Correction of the Chopper Time Offset δt

The measured TOF is the sum of the actual TOF and the chopper time offset, δt. To calculate a velocity spectrum from the observed TOF, the correct δt must be subtracted. The method to determine the value of the time offset, δt, is identical as the one described in detail in [9]. As part of this work, both methods described in [9], were carried out in Mainz. However, different guide lengths and frequencies than in [9] were used. The value for δt, found in the following analysis, is in very good agreement with the value found in [9].

4.3.5 Determination of the Time Offset δt

There are two different possibilities to determine δt: one is to measure with one fixed setup, but at different chopper frequencies; the other is to measure with the same chopper frequency, but different lengths of the flight path made of the same UCN guides. We did both measurements to be able to cross-check the results.

Frequency Variation Method:

The number of UCN counted in the detector shows a peak at a specific velocity. This peak is assumed to be at the same velocity for measurements with a given setup at different chopper frequencies. The velocity of a neutron can be calculated with an estimated value for δt:

$$v_z \;=\; \frac{L}{\mathrm{TOF} - \delta \mathrm{t}} \tag{4.3}$$

where v_z is the UCN velocity along the neutron guide axis, TOF is the measured time-of-flight, L is the flight path length and δt the offset value in question.

For different frequencies, the value of δt changes as follows:

$$\nu_{\text{Chopper}} \cdot 2\pi \quad = \quad \frac{v}{r} \tag{4.4}$$

$$with: \qquad v \quad = \quad \frac{s}{\delta t} \tag{4.5}$$

$$\delta t \quad = \quad \frac{s}{2\pi \cdot r \cdot \nu_{\text{Chopper}}} \tag{4.6}$$

$$\delta t \quad = \quad \frac{\delta t'}{\nu_{\text{Chopper}}} \tag{4.7}$$

With ν_{Chopper} being the chopper frequency, v the velocity of the part of the disc that shades the photo diode (see 3.7), r being the radius of the disc at that point and s being the distance between the point at which the diode is mounted and the point where it would have to be mounted to make the electronic signal and the actual opening coincident.

However, all these values can be neglected, as the value of δt scales with $\frac{1}{\nu_{\text{Chopper}}}$. Therefore, it is useful to determine the value of δt for a chopper frequency of 1 Hz and then use it in the formula for v_z as follows:

$$v_z \quad = \quad \frac{L}{\text{TOF} - \frac{\delta t_{1Hz}}{\nu_{\text{Chopper}}}} \tag{4.8}$$

Assuming the maximum in the velocity distribution to be the same for all frequencies, and using equation 4.8, δt_{1Hz} can be calculated as follows:
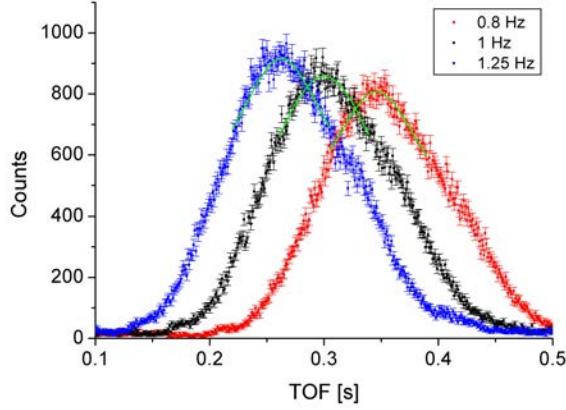
Figure 4.11: Measurements with 1 m Nocado and chopper frequencies of 0.8 Hz, 1.0 Hz, and 1.25 Hz.

$$\mathrm{v}_{max_1} = \mathrm{v}_{max_2} \tag{4.9}$$

$$\frac{\mathrm{L}}{\mathrm{TOF}_1 - \frac{\delta \mathrm{t}_{1Hz}}{\nu_1}} = \frac{\mathrm{L}}{\mathrm{TOF}_2 - \frac{\delta \mathrm{t}_{1Hz}}{\nu_2}} \tag{4.10}$$

$$\delta \mathrm{t}_{1Hz} = \frac{(\mathrm{TOF}_1 - \mathrm{TOF}_2) \cdot \nu_1 \nu_2}{\nu_1 - \nu_2} \tag{4.11}$$

where TOF_i are the TOF at the peaks of the spectra.

UCN TOF measurements were done at three different chopper frequencies, all using a 1 m Nocado tube as neutron guide between the chopper and the detector. These measurements were done at the TRIGA reactor in Mainz, using a smaller Cascade-U detector from the resident UCN group. However, this difference in detectors is negligible for the result. The peaks of the spectra were fitted with a Lorentz curve. There is no model behind the choice of the curve. Lorentz curves simply gave the best results. The data and the fits are plotted in figure 4.11 (p.61).

The peak positions obtained from the fits are shown in Table 4.1 (p.62).

Frequency [Hz]	Peak position [ms]	uncertainty from fit[ms]
0.8	349	1
1	300	2
1.25	263	2

Table 4.1: Peak positions determined at different chopper frequencies.

The values obtained for δt_{1Hz} combining the measurements with frequencies of 0.8 Hz, 1 Hz and 1.25 Hz are shown in Table 4.2 (p.62).

Used Frequencies [Hz]	δt [ms]	uncertainty [ms]
0.8 and 1	196	± 6
0.8 and 1.25	191	± 3
1 and 1.25	185	± 7

Table 4.2: δt_{1Hz} values calculated from measurements with different chopper frequencies.

It is important that the three peak values can only lead to two independent values for δt. The third value can always be obtained from the other two. Therefore, the mean of only two values (196±6 ms and 191±3 ms) is used for further analysis. The resulting mean for δt_{1Hz} is: 192±3 ms.

Length Variation Method:

Instead of altering the frequency of the chopper, one can change the length of the neutron guides between chopper and detector while keeping the chopper frequency constant. Again, it is necessary to assume that the peak of the neutron velocity distribution does not change with variation of the guide lengths. This assumption, however, will be shown to be a simplification, as the velocity distribution can change over longer distances because the UCN transmissions behavior is velocity dependent. It is therefore vital that for
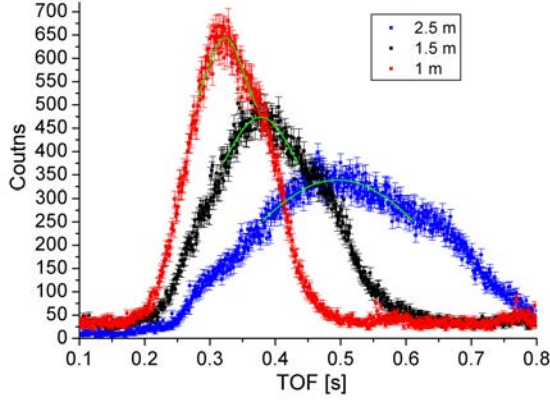
Figure 4.12: Measurements with a chopper frequency of 0.9 Hz and guide lengths of 1 m, 1.5 m, and 2.5 m of Nocado.

the length variation, identical neutron guides are used. Slits between guides should be avoided.

Using the constant peak assumption and equations 4.8 and 4.9, δt_{1Hz} is obtained as follows:

$$v_{max_1} = v_{max_2} \tag{4.12}$$

$$\frac{L_1}{TOF_1 - \delta t_{1Hz}} = \frac{L_2}{TOF_2 - \delta t_{1Hz}} \tag{4.13}$$

$$\Rightarrow \delta t_{1Hz} = \frac{L_1 \cdot TOF_2 - L_2 \cdot TOF_1}{L_1 - L_2} \tag{4.14}$$

The TOF_i are the TOF at the peak of the individual spectrum.

Three different lengths were measured: 1m , 1.5m and 2.5m[4]. All three spectra were recorded using a chopper frequency of 0.9 Hz. Unfortunately, the obtained statistics were low and the spectrum after a 2.5 m long setup is very broad. Therefore, the uncertainty on the peak position of that measurement is very large. The data and the fits are plotted in Fig. 4.12 (p.63).

---

[4]In the 2.5m measurement, the guides of the first two measurements were connected and then treated as one neutron guide with negligible slits.

Table 4.3 (p.64) shows the peak positions obtained from fits with the Lorentz distribution.

Guide length [m]	Peak position [ms]	uncertainty from fit[ms]
1	326	1
1.5	381	1
2.5	469	15

Table 4.3: Peak positions for different guide lengths.

These peak positions yield three δt_{1Hz} values shown in Table 4.4 (p. 64).

Guide lengths [m]	δt_{1Hz} [ms]	uncertainty [ms]
2.5 and 1.5	199	± 7
1.5 and 1	173	± 1
1 and 2.5	184	± 7

Table 4.4: δt_{1Hz} values calculated from measurements with different guide lengths.

The values calculated using the 2.5 m measurement have a very large uncertainty due to the lack of accuracy in the peak position. One could use the first momentum of the velocity distribution to increase accuracy, however, using the first momentum involves a different assumption for the velocity spectrum.

With the employed method, the assumption is that the peak of the velocity distribution is the same for different guide lengths, using the first momentum of the distribution is equivalent to the assumption that the shape of the entire velocity spectrum does not change for different guide lengths. As the first assumption is less restrictive, it was used for this analysis.

A Monte Carlo simulation [20] showed that for a set of realistic parameters, the peak of the velocity distribution shifts by almost 0.4 m·s^{-1} in a 2 m path through a stainless steel guide. Figure 4.13 (p.65) shows the two velocity distributions, simulated after 6 and 8 m from the source. That
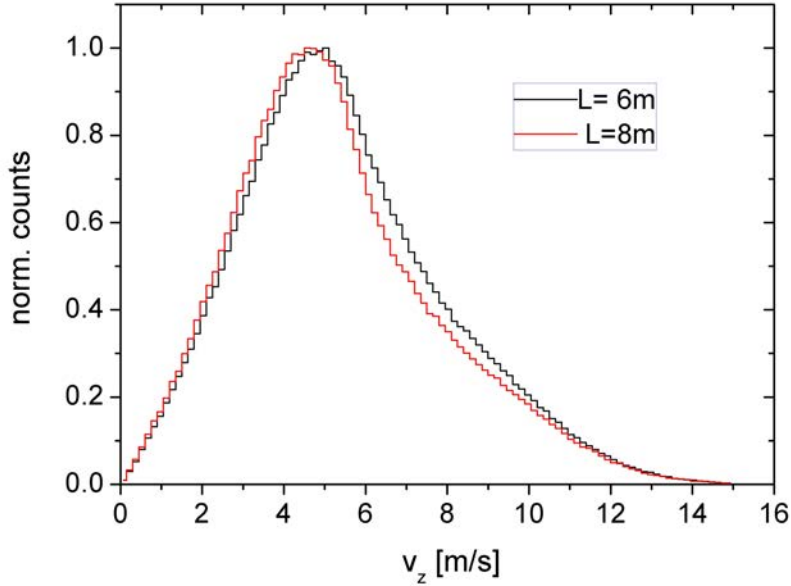
Figure 4.13: A Monte Carlo simulation of the velocity distribution after 6 and 8 m stainless steel guides with a fraction of diffusely scattered UCN of 4 %. The peaks shift by almost 0.4 m·s^{-1} [20].

simulation assumed a 4 % fraction of diffusely scattered UCN in Nocado guide tubes. It used the Mainz UCN spectrum as input and used 6 m and 8 m as guide lengths. These lengths are measured from the source, not as the previous flight path lengths, from the chopper. The chosen parameters are estimated and have a rather high diffuse scattering fraction, however, they are still within reason. The simulation suggests that the length variation is a method, that can not be used to obtain a precise value for δt_{1Hz}. Consequently, for this analysis, the weighted mean of two of the three results using the frequency variation method, $\delta t_{1Hz} = 192 \pm 3$ ms, was used[5]. The results from the length variation method were discarded in order to reduce the error.

---

[5]The value found in [9] was 191±3 ms.

4.3.6 Deconvolution of the Spectra

In the analysis part of [9], the TOF spectra are first fitted with a two-Gaussian function, as to be able to deconvolute the spectra with the opening function of the UCN chopper. The following will show why the analysis in this work employs neither the Gaussian fits, nor the deconvolution.

4.3.7 Chopper Opening Function

The chopper opens and closes the beam line by moving three rotating discs into and out of the beam (see chapter 3.7). The discs move at a constant velocity, hence changing the open beam area gradually. The assumption of a rectangular opening function would reflect an instantaneous change and is a simplification. To find out, whether that simplification is adequate or not, we measured the opening function.

We used a very simple setup consisting of the chopper, a one meter Nocado guide, and a Cascade-U detector. The chopper was rotating at a frequency of 0.1 Hz. This is slow enough that the neutrons can picture the partial covering of the beam by the discs. The obtained number of UCN counts over the measurement time reflects the opening function which can then easily be scaled to all rotation frequencies. Figure 4.14 shows the result of that measurement as a function of time. The distribution has roughly rectangular shape, however, a trapezoid is a better approximation. The ratio of the area under the rising and falling slope to the area under the constant plateau is 0.70±0.05. Calculations have shown (see below) that both a rectangular and a trapezoid approximation of the opening function lead to similar results.

Before having measured the shape of the opening function to this accuracy, a study was performed on the influence of the deconvolution of the
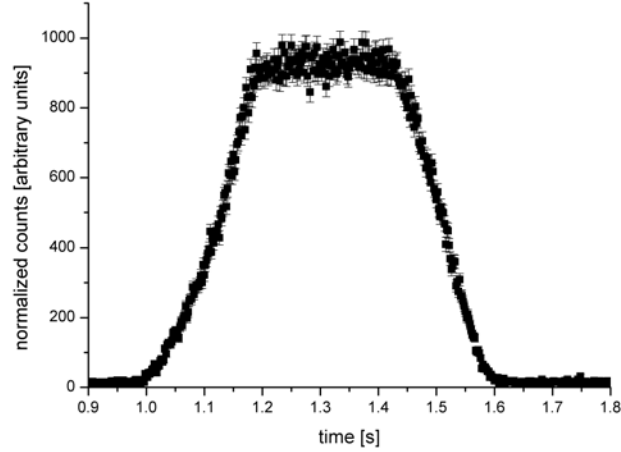
Figure 4.14: The opening function of the UCN chopper, measured with 0.1 Hz and a 1 m guide between chopper and detector

TOF spectrum with the opening function. Then, a rectangular function with a width of 0.055 s was used at a chopper frequency of 1 Hz. The impact on the experimental data for UCN between 3.3 and 6 m·s^{-1} turned out to be negligible within the statistical error of the measurement.

After measurement of the opening function in Mainz, the deconvolution was performed by the UCN group in Mainz using a trapezoid as an opening function. This again turned out to have negligible effect on the UCN region. As an example, figure 4.15 (p.68) shows a TOF spectrum measured in Mainz and the result of the deconvolution with the trapezoid. There is no significant deviation of the two spectra within the UCN region. The integrals from 3.3 to 6 m·s^{-1} agree within the statistical error. The deconvolution of the TOF spectra has a small influence on the fast side of the spectrum ($v_z > 10$ m·s^{-1}). However, the effect on the UCN region analyzed here is so small that it was neglected.
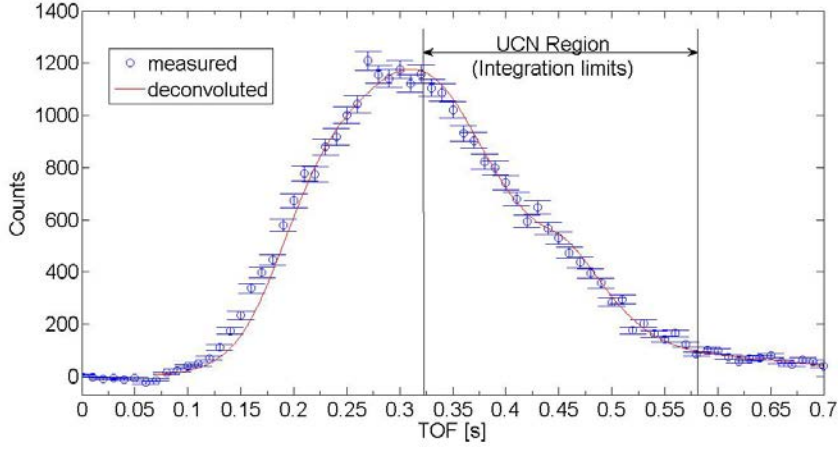
Figure 4.15: Measured TOF spectrum compared with its deconvolution. The two curves show a deviation on the fast side of the spectrum, the difference in the UCN region indicated by the vertical lines is negligible.

4.3.8 Conversion from TOF to v_z Spectrum

The conversion from a $\frac{dN}{dTOF}$ (TOF) to a $\frac{dN}{dv_z}$ (v_z) distribution is done as follows:

$$\frac{dN}{dTOF} \longrightarrow \frac{dN}{dv_z}$$

$$\frac{dN}{dTOF} \cdot \frac{dTOF}{dv_z} = \frac{dN}{dv_z} \tag{4.15}$$

$$\text{using:} \quad TOF = \frac{L}{v_z} \tag{4.16}$$

$$\frac{dTOF}{dv_z} = -\frac{L}{v_z^2} \tag{4.17}$$

$$\Rightarrow \frac{dN}{dv_z} = -\frac{dN}{dTOF} \cdot \frac{L}{v_z^2}. \tag{4.18}$$

Where TOF is the time-of-flight, v_z the velocity in direction of the guide axis and L the distance between chopper and detector.

To obtain the spectrum $\frac{dN}{dv_z}$, one converts the x-axis by dividing the distance L by the TOF and one converts the amplitude by multiplying the values by $\frac{L}{v_z^2}$, using the individual v_z.

The comparison of a TOF and a v_z spectrum is shown in Fig. 4.16 (p.69).

68

(a) TOF spectrum.
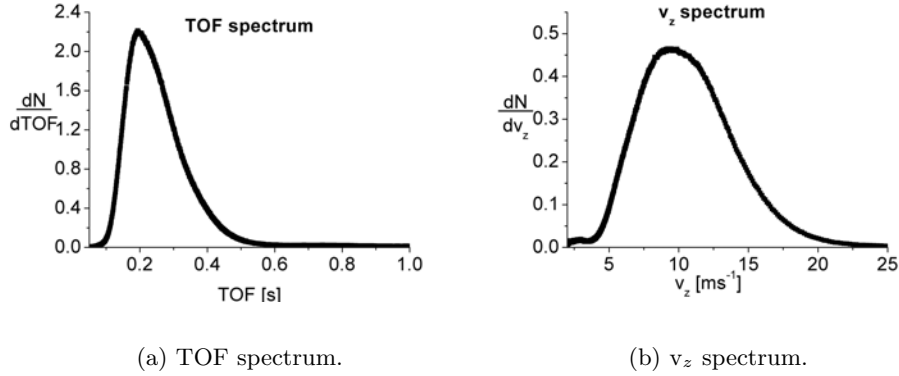
(b) v_z spectrum.

Figure 4.16: Comparison of a TOF spectrum and corresponding v_z spectrum measured at ILL.

For a comparison of the velocity distributions in Mainz and at ILL see figure 4.20 (p.79).

4.3.9 Definition of Transmission and Integral Boundaries

The aim of the TOF measurement is to provide a value for the UCN transmission of a given UCN guide in a given velocity interval. To do that, integral count rates for these intervals in the two setups are necessary. These are calculated by summing up all counts in the TOF channels between the two TOF corresponding to the boundary velocities.

Example:

To provide a transmission value for the velocity interval $v_1 = 3.3$ m·s^{-1} to $v_2 = 6$ m·s^{-1}, these two speeds are converted into TOF using $TOF = \frac{L}{v_z}$. The two corresponding TOF for a hypothetical setup with a length of 2.2m would be $TOF_1 = 0.67$ s and $TOF_2 = 0.37$ s. The minus sign mentioned in 4.17 (p.68) inverses the integration limits, i.e., the integral goes from 0.37 s to 0.67 s.

Summing up the count rates of the "corrected" (see 4.3.4) TOF channels between these two limits gives the count rate of the interval. This integration is done for both, the measurement with the test guide and the one without it.

To obtain the transmission for the UCN guide, the integral count rates are divided by each other.

$$
T_g \;=\; \frac{\displaystyle\int_{TOF(v_{z,1})}^{TOF(v_{z,2})} \frac{\mathrm{dN_1}}{\mathrm{dTOF}}\,\mathrm{dTOF}}{\displaystyle\int_{TOF(v_{z,1})}^{TOF(v_{z,2})} \frac{\mathrm{dN_2}}{\mathrm{dTOF}}\,\mathrm{dTOF}}. \tag{4.19}
$$

Where T_g is the UCN transmission of the guide, and the integrals are the integrated count rates.

In this analysis, the boundary velocities were usually chosen to be 3.3 m·s^{-1} and 6 m·s^{-1}. The lower boundary is a limitation from the aluminum foils in the setup (UCN source window, detector window), the critical velocity of aluminum being 3.22 m·s^{-1}. The upper bound is given by the expected maximum velocity spectrum coming from the storage volume at the PSI source. For historical reasons, the boundary is set to 6 and not to 6.8 m·s^{-1} as one might expect from the simulation. See Fig. 4.17 (p.71) for a simulated spectrum expected in the UCN guides at PSI.

For better comparability, it is useful to define a transmission per unit length. Assuming the guide properties are exactly the same all along the guide and using a as the multiple of the unit length 1 m, this value can be calculated as follows:
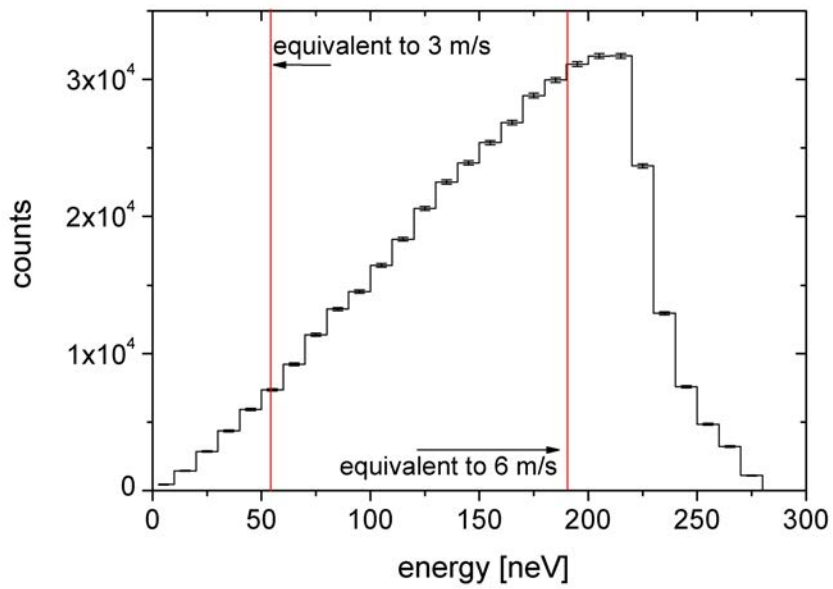
Figure 4.17: UCN energy spectrum expected in the UCN guides at the PSI source. The horizontal lines indicate the integration boundaries. Spectrum from [20]

$$N(a) = N_0 \cdot T_g = N_0 \cdot T^a \qquad (4.20)$$

$$\Rightarrow T = \sqrt[a]{T_g} \qquad (4.21)$$

We call the transmission calculated following eq. 4.20 and using the total BG described in section 4.3.2 "direct transmission". It represents the transmission for UCN which have only undergone specular reflections. Diffusely scattered UCN are not necessarily lost but can reach the detector after a longer travel time. Therefore, the direct transmission gives a lower bound on the total UCN transmission. If not commented differently, this formula is used for all transmission values presented in this thesis.

4.3.10 L.A.E.P.C.

Analysis is sometimes a lengthy task, that is why the repetitive work should be left to computers. This yields a better reliability and the ability to reconstruct all performed calculations easily. In order to evaluate the measurements done with the Cascade-U or the ^{3}He-counter, I wrote several macros in the MATLAB environment. As it was my first program to evaluate data, I called it "Lenny's Attempt for an Evaluation Program", hence L.A.E.P.. There are two versions of the program, one for Cascade (L.A.E.P.C.) and one for the ^{3}He-counter (L.A.E.P.H.), as the two detector signals are recorded with different DAQ systems and, hence, the output files have different formats.

The main functions of the program are the same for both versions, however, the L.A.E.P.C. has one parameter more. As mentioned in the hardware-chapter, the Cascade-U has a spatial resolution because of its pixel

read-out structure, therefore, it is possible to select certain pixels (more detail in section 4.3.11, p.73). After summing up the selected pixels, both programs do the same, following the steps described in the previous sections, namely:

- remove sparks and noisy channels;

- fit and subtract a background value;

- convert the counts to a count rate, via normalization to the measurement time;

- integrate the count rate over a selected velocity range;

- write a log-file, containing the integral count rate and the count rate vs. TOF data.

The calculation of the transmission value itself is left to the user.

4.3.11   Pixel analysis

The L.A.E.P. program can be used for pixel analysis of the Cascade-U detector data. The goal of this analysis is to reduce background. The detector has a total of 256 pixels of which only a part is exposed to UCN. The active detector area is a square with 200 mm side length, the UCN guides used have diameters between 70 and 180 mm. This means that the pixels in the corners are never exposed to UCN. One can easily see the shape of the used guide in Fig. 4.18 (p.75).

Figure 4.19 shows the TOF spectra of the two pixel groups for a 1 m Nocado tube measurement. The signal-to-BG ratio for the valid pixels is 4.7 to 1, the one for the outer pixels, discarded in the analysis is 2.9 to 1 [6].

---

[6]Signal-to-BG : maximum signal height to maximum BG height

The pixels marked in red on Fig. 4.18 are hence excluded from the analysis.

4.4 Uncertainties of the TOF Method

Now that we have calculated the transmission of the UCN guide, the question of uncertainties arises. How reliable is the obtained value and how accurate is it?

4.4.1 Statistical Error

To calculate transmission values, that have a small statistical error (1-3% error in the selected velocity interval) one needs to detect $\sim 100\,000$ UCN in the entire spectrum. With UCN rates of 50 Hz (Mainz), this corresponds to a measurement time of ~ 2000 seconds. Preparations for the final guide tests have to consider the duration of the measurements, so it must be known in advance. At ILL, we measured neutron rates of 1kHz but the beam has a velocity distribution peaked towards higher velocities than the source in Mainz (see Fig. 4.20, p.79), i.e., the mean UCN velocity is also higher.

In a transmission measurement with a total of N counts in the selected velocity interval, the statistical error was taken to be $\sqrt{N}$. The statistical error of the transmission was then calculated using Gaussian error propagation.

4.4.2 Error due to the Uncertainty of the Setup Length

The boundaries of the two integrals to calculate the transmission (Eq. 4.19) are velocities converted into TOF. The conversion is a simple division of
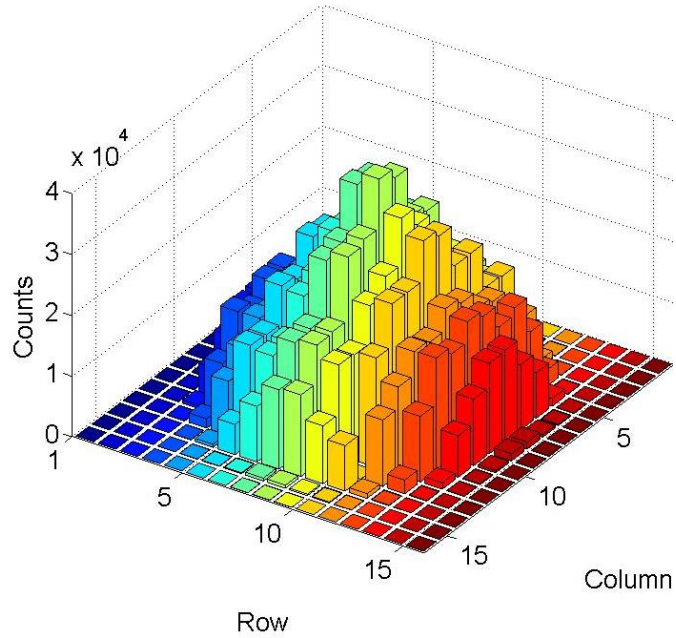
(a) Counts versus individual pixel. The profile reflects the shape of the guide tube. The low number of counts on the outer pixels is due to shielding by the flange and the size of the guide tube, which is smaller than the detector.

(b) Pixel map of the Cascade-U detector, the numbers in the cells are "pixel ID". Red (dark) pixels are regarded as background dominated and excluded from the evaluation to increase the signal-to-noise ratio.

Figure 4.18: Position dependence of UCN counts observed with the Cascade-U detector at ILL.
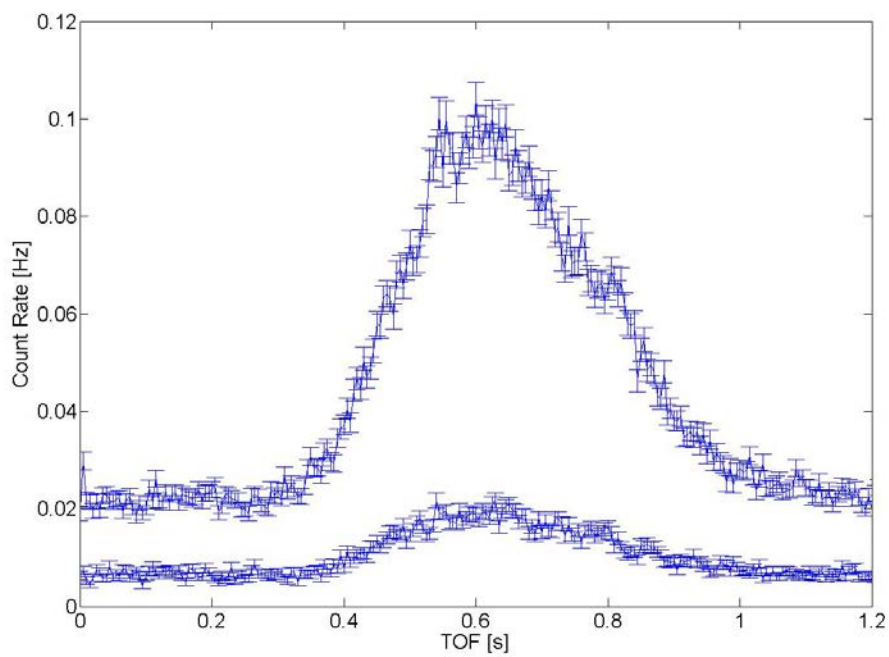
Figure 4.19: TOF spectrum of a 1 m guide divided into the two pixel groups. Lower curve: the outer pixels, neglected in the analysis. Higher curve: center pixels, evaluated in the analysis.

76

the flight path length by the velocity. That, however, means that the uncertainty on the flight path length directly translates to an uncertainty in the boundaries of the integral. A conservative uncertainty of ± 3 mm per meter guide was assumed. This is estimated to be the reproducibility of the connections between the used tubes, which, if not connected perfectly, will have small slits. However, the magnitude of the error on the transmission arising from the uncertainty on the length also depends on the source. At ILL, the impact is higher than in Mainz. The reason for that are the different velocity distributions of the two sources. This will be explained in detail in section 4.4.3.

Measurements with the ^{3}He counter have an additional uncertainty on the flight path, as the mean free path of UCN with velocities between 4.5 m/s and 6 m/s in the ^{3}He detector, is 10 ± 4 mm. The distance uncertainty originates from the uncertainty on the position of the detection reaction which occurs in a gas volume with a length of $\sim$4cm. The position of the conversion reaction can be determined more accurately [9]. The Cascade-U detector has a 100 μm thick boron layer, in which the conversion takes place. This reduces the error on the position of the detection reaction by a factor of 100.

4.4.3 Error due to the Uncertainty on the Chopper Time Offset δt

In the analysis, the TOF spectra have to be shifted by a time offset with value δt (see chapter 4.3.4, p.59). An uncertainty on δt translates to an uncertainty on the integration boundaries. The determination of δt is described in detail in chapter 4.3.5 (p.59). The uncertainty on the value of δt is $\sim$1.5 percent, but small variations of the integral boundary velocities have a large impact

on the value of the integral.

The error in the transmission value resulting from the uncertainty on δt depends on all parameters entering the determination of the UCN velocity, namely the guide lengths, the chopper frequency, and mostly on the UCN velocity spectrum. The magnitude of the error resulting from the uncertainty in δt decreases with increasing distance from the chopper to the detector.

The integral count rate at ILL is very sensitive to an uncertainty in δt because the velocity spectrum of the test beam has its peak at around 10 m·s^{-1} (see Fig. 4.20, p. 79), which means that the slope of the spectrum is very steep at the upper velocity boundary (6 m·s^{-1}), i.e., a small change in v_z translates in a larger change in the transmission.

In Mainz, using the experimental setup half a meter over the beam, - see chapter 4.2 (p.50) - the spectrum has its peak around 6 m·s^{-1}. The slope of the spectrum at the upper boundary is close to zero This reduces the error of the integral dramatically.

The error due to δt was calculated by using the maximum and minimum values for δt in the analysis. At ILL, the error on T due to the uncertainty in δt is between 0.03 and 0.09, in Mainz, due to the different spectrum, this uncertainty is reduced to 0.01. The uncertainties given are expressed in terms of UCN transmission.

4.4.4 Time Resolution of the DAQ System

If the DAQ system is set to an acquisition rate of 1 kHz or more, the uncertainty resulting from the detector DAQ is negligible as that rate means a time resolution of a millisecond or less.
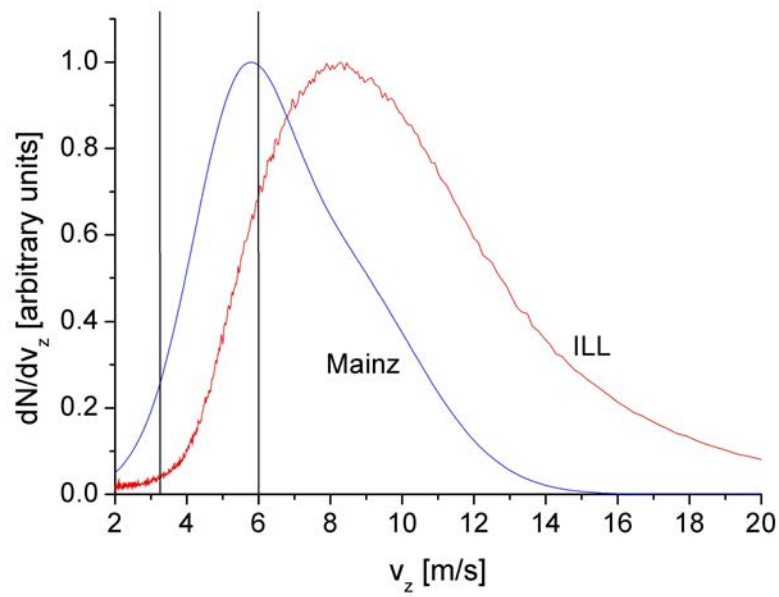
Figure 4.20: Boundary velocities 3.3 and 6 m·s^{-1} indicated by vertical black lines. Notice the position of the higher velocity, which is an integration boundary. The steep slope at this position is the reason for the high sensitivity of T to the uncertainties on L and δt. The graph shows the velocity distributions in Mainz and at ILL. The maximum intensities are both normalized to 1.
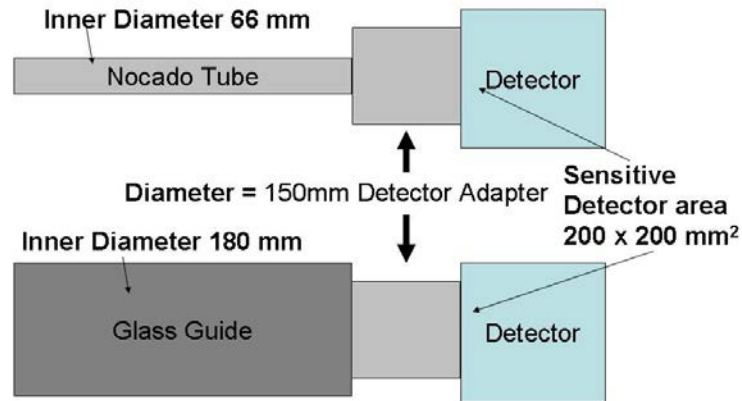
4.4.5   Geometric Consideration

Figure 4.21: The top shows the setup for the measurement without the glass, the bottom the measurement with the glass

The guide test experiments were done with the Cascade-U detector. Due to technical reasons, a 20 cm stainless steel tube with an inner diameter of 150 mm was used as adapter flange. The measurement without the glass was done flanging a stainless steel guide with 66 mm inner diameter to the tube. The glass guides have an inner diameter of 180 mm. That means, we are in fact cutting away parts of the counts in the glass measurement because the opening to the detector is smaller than the tube (See figures 4.21 p.80 and 4.22 p.81).

We have used two different approaches to determine this geometric correction factor.
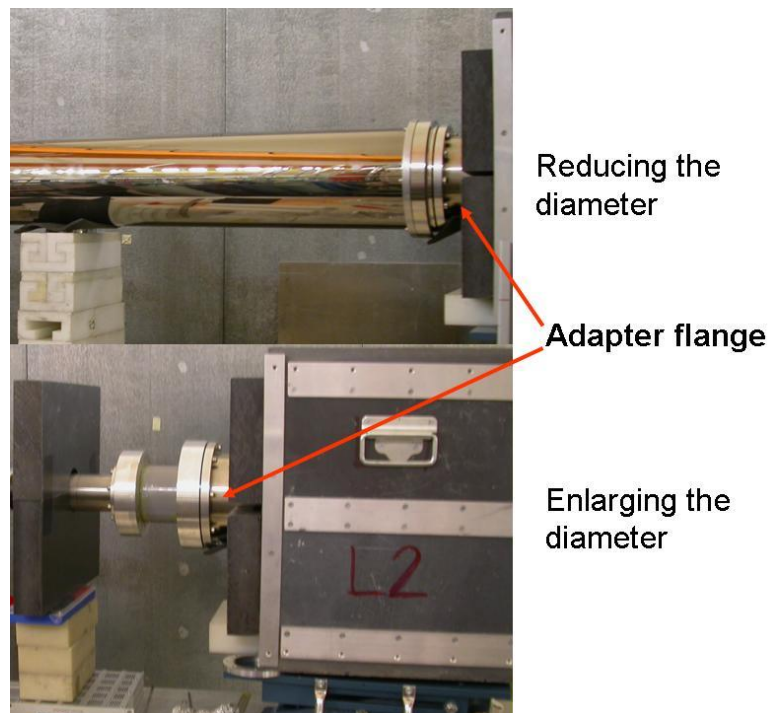
Figure 4.22: Pictures of the two setups at ILL, the flange indicated by red arrows.

Via the Shape of the UCN Distribution

The UCN count distribution (Fig. 4.18) is peaked in the center. Investigating the energy dependance of this distribution unveils an even stronger peaking in the center for higher velocities shown in Fig. 4.23 (p.82).

Considering the radial neutron density distribution to be similar in a 150 mm diameter and a 180 mm tube, it is possible to find a correction factor for the lost counts. The second assumption is, that this radial distribution is achieved after only 20 cm of path length in a UCN guide. Both assumptions might be oversimplifications. One can refine the result by using two energy intervals, UCN and VCN, with 7 m·s^{-1} being the boundary velocity (see Fig. 4.23 p. 82).
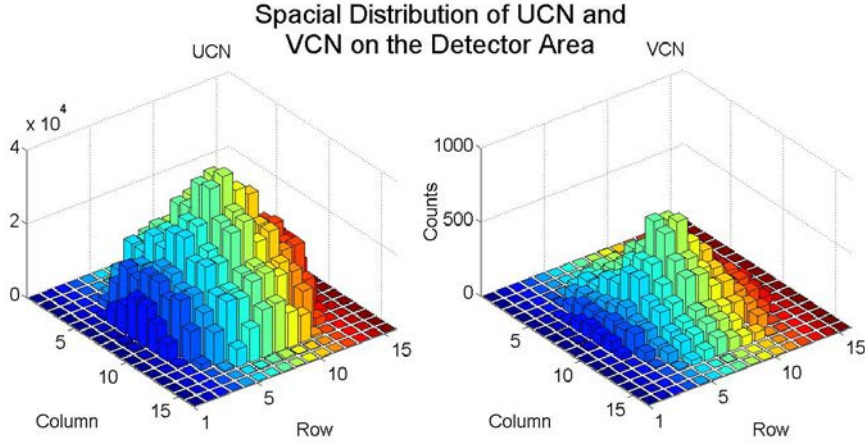
Figure 4.23: The VCN are more peaked in the guide center than the UCN. Therefore the geometric correction factor should be calculated for UCN only.

The x-axis of the radial UCN density distribution in a 150 mm tube was scaled to 180 mm diameter and the counts in the outer pixel ring (see Fig. 4.18 p. 75) were summed. The scaling factor was obtained by dividing the two diameters:

$$\frac{150\text{mm}}{180\text{mm}} \; = \; 0.833 \; . \tag{4.22}$$

The ring shaded by the reducing flange has a width of 15 mm. Scaling that with the factor of 0.833 gives a width of 12.5 mm, which coincidentally is the width of one pixel (see Fig. 4.24). By integrating the UCN count rate over all pixels and comparing that to the integral just over the area not covered by the ring for four different measurements, I found that 21 % of the UCN were located in this outer ring, i.e., 79 % are detected which means the geometric correction factor has to be calculated as follows:

82

$$C_{geo} = \frac{1}{0.79} = 1.27. \tag{4.23}$$

The uncertainty was estimated in the following way: every individual pixel has a large cross section (12.5 mm x 12.5 mm), and some pixels are only partially covered by this ring. We took all the partially covered pixels, added their counts to the counts in the fully covered pixels for the upper boundary, and considered just the fully covered pixels for the lower boundary. Investigating the hit distribution at different velocities shows a negligible dependence on the exact value of the boundary velocity. This leads to an uncertainty of 7 % on the fraction of UCN in the outer ring. This translates to an error of 0.12 for C_{geo}.

This leads to $C_{geo} = 1.27\pm0.12$ due to the non-matching of the guide diameters.
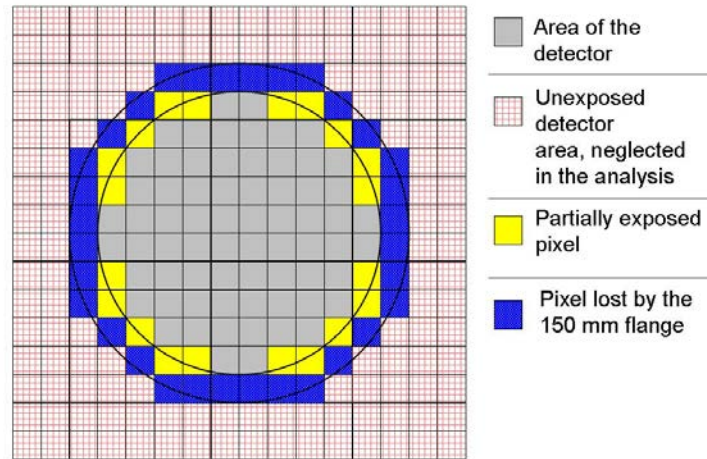

Figure 4.24: The picture shows a pixel map of the Cascade-U detector. The two guide diameters, 180 mm and 150 mm, are indicated by solid lines.

Via Comparison of Transmission Values Obtained with Different Measurements

At ILL, measurements with no test guide, one test guide, and two test guides were done. Figure 4.25 (p.84) illustrates this. Using the measurements with guides 1 and 2, one can calculate the transmission of guide 1 (T_{guide1}) without using a correction factor, because in both measurements the loss on the reducing flange is the same fraction of the UCN flux, assuming the radial distribution stays the same after one and after two test guides. The transmission of guide 1 can also be measured with the standard setup shown in figure 4.25, $T_{guide1}*$. The two values T_{Guide1} and $T_{Guide1}*$ should be the
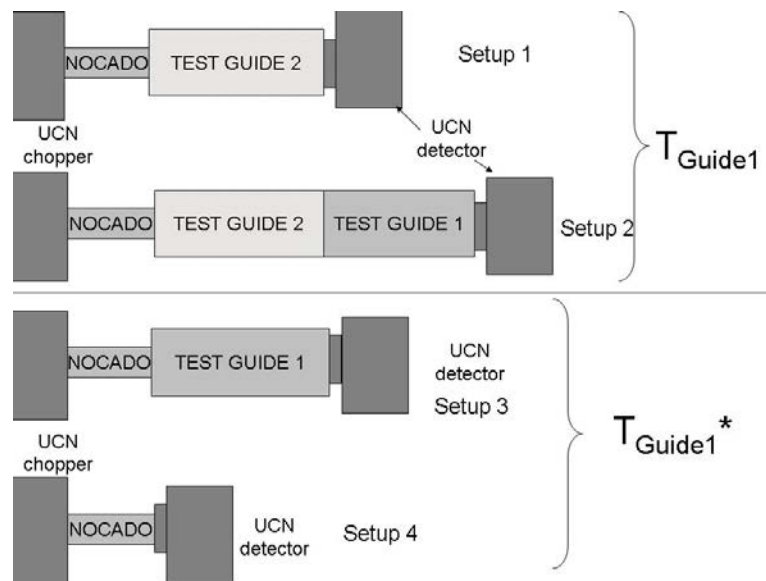

Figure 4.25: The four setups needed to find the correction factor for the reducing flange.

same. The geometric correction factor can be calculated as follows:

$$C_{geo} \;=\; \frac{T_{\text{Guide 1}}}{T_{\text{Guide 1*}}} \tag{4.24}$$

In this case, the correction factor was determined to be $C_{\text{geo}} = 1.11 \pm 0.14$.

Both approaches agree within the error. However, the first approach involves a strong simplification. Therefore, the correction factor used for the calculation of the transmission values of the test guides with a diameter of 180 mm was taken from the second approach.

There is always a relative error contribution of 0.13 to the systematic error of the transmission.

4.4.6   Summary of the Uncertainties

The following uncertainties were considered:

1. Statistics (1 - 3 %).

2. Length of the flight path (0.3 %).

3. Time resolution originating from detector and DAQ (< 1 %).

4. Geometric considerations[7]($\sim$15 %).

5. The time offset δt (2 - 10 %).

The geometric factor is the dominant uncertainty for this analysis but in the final guide test measurements, the setup will be different and C_{geo}, therefore, not necessary. The uncertainty on the value of δt has to be reduced in order to obtain precise transmission results (systematic error smaller than 5%).

---

[7]The geometric correction was only applied for the 180 mm glass tubes.

4.5 Results

4.5.1 Steel UCN Guides

In January 2008, we measured the transmission of 66 mm inner diameter stainless steel Nocado tubes, which are frequently referred to as "standard UCN guides", and of stainless steel guides with an inner diameter similar to the Nocado tubes. The latter tubes made in Japan had undergone a special polishing - electrochemical buffing[8] - in a Japanese company (Ultra Finishing Technology). Optically, the Japanese tubes seemed to be of superior quality: The surface was shiny and seemed less wavy. Looking at the surface with an atomic force microscope (AFM) reveals that both tubes have similar roughness values, however, the Japanese tube shows grooves perpendicular to the tube axis (see Fig. 4.26, p.87). The UCN transmission was significantly higher in the Nocado tubes. The results are shown in table 4.5 (p.86). A likely reason for this are the grooves perpendicular to the guide axis in the Japanese tubes.

UCN guide	Inner diameter [mm]	Transmission $[\mathrm{m}^{-1}]$	statistical error	systematic error
Nocado	66	0.82	± 0.02	± 0.01
Japanese	66	0.70	± 0.02	± 0.01

Table 4.5: Results for transmission of Nocado and Japanese tubes.

Thus, although the guides looked better to the naked eye, UCN-measurements found the Nocado tubes to be superior. The idea to ship all steel parts included in the PSI UCN source guide system to Japan for a polish was discarded because of the results from this transmission measurement.

---

[8] A special polishing technique that combines electrochemical with a mechanical polishing with an abrasive. For more detail see `http://www.uft.co.jp/english/index.html`
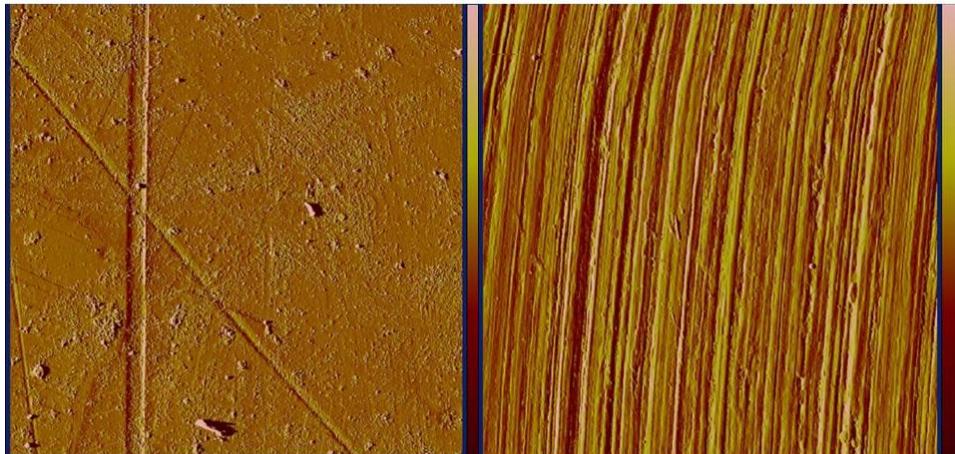
Figure 4.26: AFM pictures of small samples of the two stainless steel tube types; Nocado and polished via electrochemical buffing.

4.5.2 Glass Guides

Measurements were done with three identical glass tubes differently treated before the coating process. Tube number one was coated without having undergone the cleaning procedure developed at PSI. The other two tubes were cleaned with procedures described in chapter 3.1.3 (p.22), i.e., one was cleaned by hand (measured in four configurations), the other was cleaned in a professional edging facility (tube HF).

The uncleaned guide had obvious coating defects. There were holes and streaks in the coating. To the naked eye there was no visible difference in the coating quality of the two cleaned guides. Both had a small amount of tiny holes in the coating, visible only when light was shining through. The number and size of holes in the clean guides was several orders of magnitude smaller than in the uncleaned guide. The measured transmission values are shown in table 4.6 (p.88).

UCN guide	Inner Diameter [mm]	Transmission [m^{-1}]	Corr. Transmission [m^{-1}]
Uncleaned Guide	180	0.66±0.01±0.01	0.73±0.10
HF-Edged Guide	180	0.67±0.04±0.03	0.73±0.17
Hand-washed Guide 1	180	0.75±0.04±0.04	0.82±0.19
Hand-washed Guide 2	180	0.74±0.04±0.04	0.82±0.19
Hand-washed Guide 3	180	0.81±0.01±0.04	
Hand-washed Guide 4	180	0.82±0.01±0.04	

Table 4.6: Results for the glass guides, the result for the unwashed guides is calculated from a measurement in Mainz, the others are calculated from measurements at ILL. The errors given are the systematic and the statistical error, respectively. Hand-washed 1-4 as explained in the text. Hand-washed 3 and 4 were measured after the HF-edged guide, hence C_{geo} was not applied to the transmission value.

In Table 4.6, Corr. Transmission stands for the transmission using the

geometric correction factor of 1.11±0.14. The four results for the hand washed guide were measured as follows.

1. Measured after 1 m Nocado.

2. Measured after 1 m Nocado but turned by 180° compared to measurement 1.

3. Measured after 1m Nocado and 1 m HF-edged glass guide. The guides were not aligned properly, there was a ∼2° bend between the HF-edged and the hand washed guide.

4. Like in measurement 3 but with a bend of less than 1°.

The uncleaned guide was measured in Mainz, the other two at ILL. It is, therefore, difficult to compare the transmission values. The velocity distribution at ILL has a very steep slope in the integration interval, i.e., the mean velocity is higher than in the same interval in Mainz. This means, that the UCN transmission for 3.3 to 6 m·s^{-1} UCN will be better in Mainz than at ILL for the same guide. It has not yet been possible to determine that difference accurately.

The hand-washed guide had the best UCN transmission of all tested tubes. This measurement was used to select the process which will be applied for the final UCN guides at PSI.

4.5.3 Comparison with Literature Values

Both the stainless steel guides and the glass test guides might yield seemingly low transmission values compared to literature, e.g. [10] gives transmissions per unit length of 0.9 for an electrolytically polished stainless steel guide with an inner diameter of 66 mm. However, these values result from different measuring methods.

Typically, results for UCN guide transmission are based on an integrated count rate of UCN. The velocity selection is done, using a UCN filter (e.g. a U shaped guide) instead of a chopper. Those measurements are done with a continuous UCN source, filling the guide during the whole measurement. This makes it impossible to distinguish the contribution of diffusely and specularly scattered UCN to the integral count rate. As we analyze only the specularly scattered, the transmission we find is intrinsically smaller. Therefore, a direct comparison between our transmission values to the ones cited in [10] is not possible.

Chapter 5

Transmission Measurements Using UCN Pre-Storage

For transmission measurements, an alternative approach to TOF is to use a UCN pre-storage volume. If neutrons are stored, the VCN and neutrons of higher energies leave the storage vessel, the UCN are trapped inside. By choosing a long enough storage time, it is possible to filter the UCN out of the neutron beam.

Using the TOF method, the UCN are selected by their measured v_z, here they are selected by storage properties. Therefore, the two methods are sensitive to different systematic errors.

5.1   Measurement Principle

Figure 5.1 shows a scheme of the transmission measurement with pre-storage of UCN.

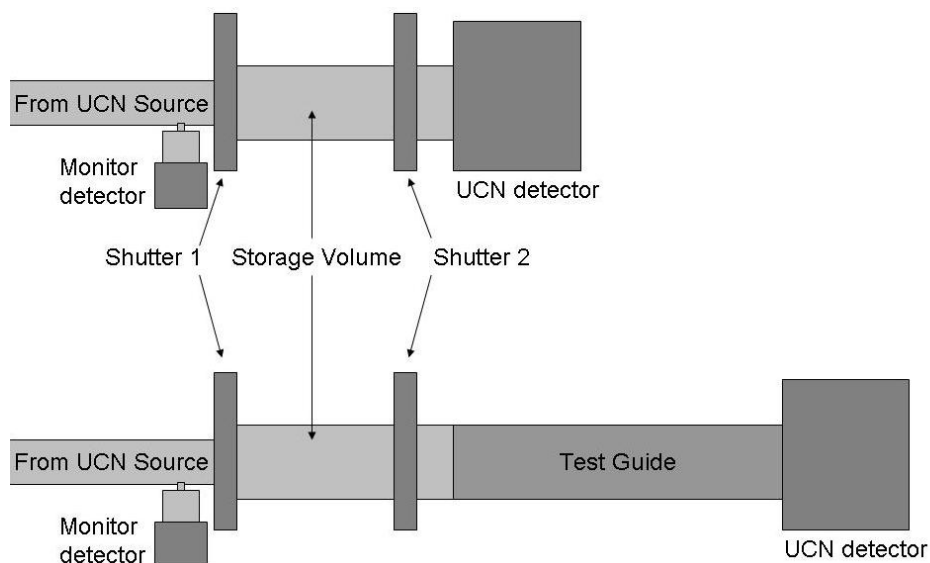Firstly, the neutrons enter the storage volume through the open shutter

Figure 5.1: Top: Setup without the test guide. Bottom: setup with the test guide. The storage volume is used to make sure that the neutrons detected at the end of the setup are UCN and not faster neutrons.

1 while shutter 2 is closed. After the "closing time", i.e., as soon as the neutron density inside the storage vessel has reached its maximum, shutter 1 is closed. After a trapping time that is long enough to isolate the UCN from faster neutrons, but still short enough not to loose too many UCN, shutter 2 is opened, and the neutrons are counted. This procedure is done with and without the test guide.

5.2 Lab Situation

In Mainz, the pre-storage measurements were done running the reactor in pulsed mode. The reactor pulses initialize a TTL signal which can start a measurement, analogous to the chopper signal in TOF measurements.

To maximize the number of stored UCN per pulse, it is necessary to find the optimal closing time. As the reactor is in pulsed mode, so is the UCN source. Therefore, shutter 1 should be closed, after the UCN pulse
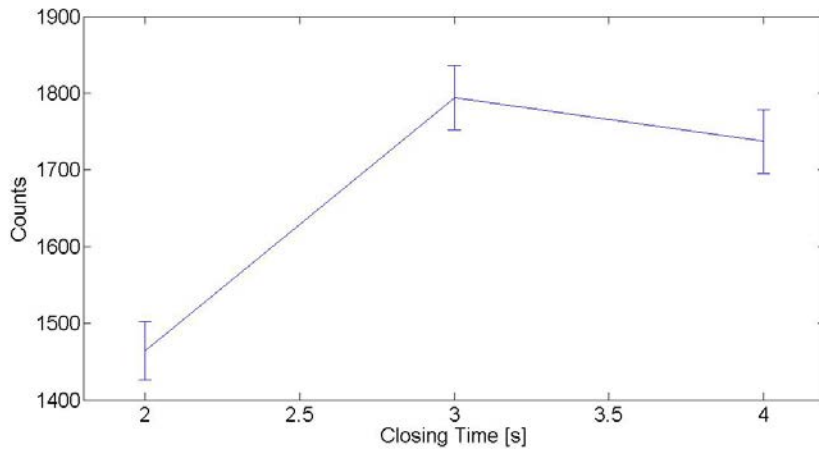
Figure 5.2: UCN counts for different closing times using 2 s trapping time.

has entered the storage vessel but before the UCN can exit the vessel again. To find the right closing time, the trapping time is kept constant and the closing time is varied. The closing time yielding the highest number of UCN is then used for the pre-storage measurements. The used closing time and trapping time were both 3 s. The optimization of the closing time is shown in figure 5.2 (p.93

The difference between the pre-storage measurement and the chopper measurement is that although both work with "pulses", the pre-storage delivers a long pulse, due to the emptying time of the pre-storage vessel which is significantly larger than the chopper pulse, and depends on the size of the pre-storage volume, the storage time and the emptying hole. Thus, it is not as easy to distinguish between the specularly and the diffusely scattered UCN. With some further development of the method and higher statistics, it might be possible to separate the two groups of UCN by two time constants
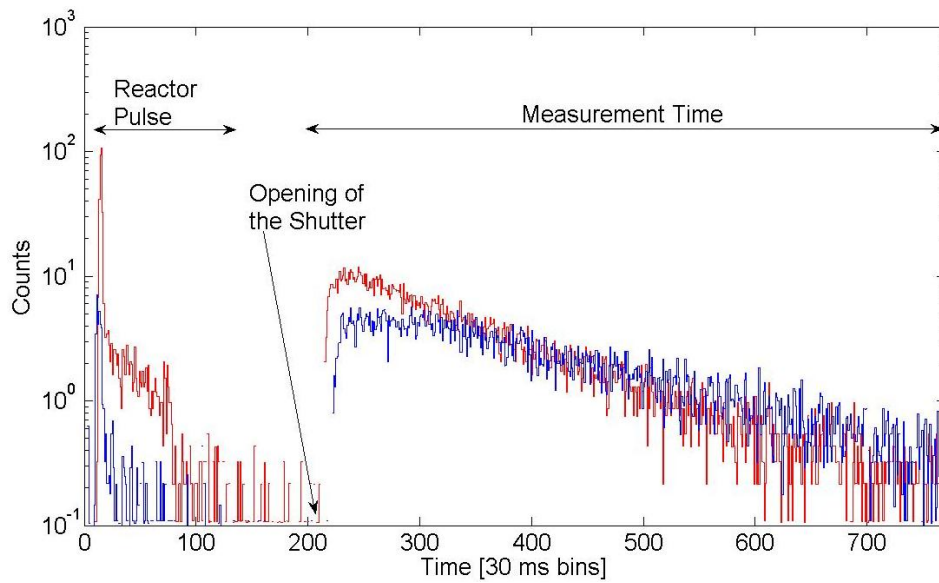
Figure 5.3: Pre-Storage experiment done in Mainz, April 2008. The red curve was measured without the guide, the blue one with the guide in the beam line. The first peak is caused by the reactor pulse, the second is caused by UCN after opening shutter 2. For this graph, the two measurements were shifted so the actual measurement would start in the same bin. Would we shift the spectra to have the reactor pulse in the same bin, one could see a slight delay of the measurement with the guide due to the longer flight path. The longer distance from the source is also the reason for the lower reactor pulse signal in the measurement with the guide.

in the spectrum. The specularly reflected UCN have a shorter TOF than those that were diffusely scattered.

Using a continuous UCN source like the turbine at ILL, the closing time has to be found using a similar technique. Instead of trapping as much of the UCN bunch in the storage vessel, one needs to find the correct filling time. After opening shutter 1, the density of UCN in the storage vessel rises until an equilibrium situation is reached. However, due to lack of beam time, no pre-storage or storage measurements using continuous UCN sources have been done during this thesis.

5.3 Analysis

The guide used in the experiment was the uncleaned guide, thus the bad transmission. The analysis of the pre-storage measurement (see 5, p.91) is simple as far as the transmission value is concerned. The normalized sum of the UCN counts of the measurement with the mounted glass guide (C_{with}) is divided by the normalized count sum of that without the test guide ($C_{without}$). The transmission T_{PS} can again be given per unit length:

$$T_{PS} \;=\; \sqrt[L]{\frac{\Sigma C_{with}}{\Sigma C_{without}}} \tag{5.1}$$

where L is the length of the analyzed guide.

The individual measurements are normalized to the delivered pulse power, which is monitored by the reactor crew. They state the pulse power with an accuracy of $\sim$0.1 MW per pulse.

We measured 5 pulses with each setup. Figure 5.3 (p. 94) shows the two sum-spectra.

5.4 Results

Table 5.1 (p.96) shows details for the actual measurement part of the two summed spectra.

Measurement	Total Power [MW]	Counts
With glass guide	46.4±0.2	1150±34
Without glass guide	46.3±0.2	1485±39

Table 5.1: Total reactor power and integral counts for the summed spectra. The error on the counts is the statistic error only.

We found the uncleaned glass guide to have a transmission of 0.77±0.05 m^{-1}. The uncertainty is composed of the statistical uncertainty and the pulse power uncertainty.

5.4.1 UCN Energy Distribution

The spectrum of UCN that leave a stainless steel pre-storage vessel was simulated in [20]. Figure 5.4 (p.97) shows the velocity distribution of UCN leaving the pre-storage vessel after storage times of 1 and 5 seconds. The spectrum of the Mainz UCN source - after a raise of the beam by 0.5 m - was used as input for the pre-storage vessel. The velocity spectrum is ideal for our purposes, as almost all UCN have velocities between 3.3 and 6 m·s^{-1}. This distribution can be compared to the ones determined for Mainz and ILL (see Fig. 4.20, p.79) from TOF measurements.
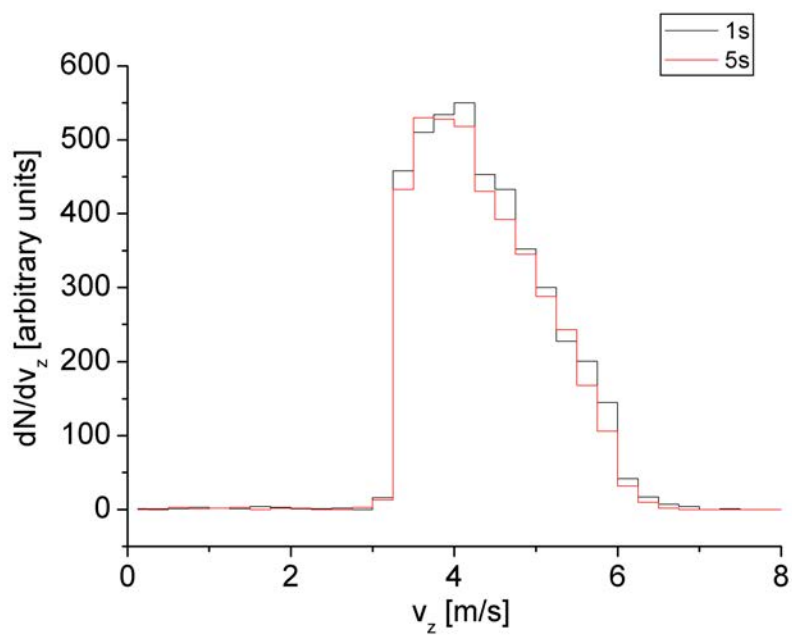
Figure 5.4: Simulated velocity distributions after storage times of 1 and 5 seconds in the pre-storage vessel. The Mainz UCN source spectrum after a raise of the beam by 0.5 m was used as input for the pre-storage vessel.

Chapter 6

Foil Transmission

Aluminium foils are used as vacuum windows in many UCN experiments. At PSI, the end windows of the UCN source have to close the source safety vacuum, which is the volume that would be filled with deuterium, in case the moderator would leak and the solid D_2 would become gaseous. However, these end windows also have to transmit the UCN on the way to the experiments. Thus, a high UCN transmission is required. To meet these needs, a 100 μm thick aluminium foil is used as end window. As there are many different alloys of aluminium, transmission measurements were done to find the foil with the best UCN transmission properties. In addition (in cooperation with the PSI vacuum group), burst tests [21] were conducted with all foils to find out, whether the foils meet the safety requirements, i.e., the foil has to withstand more than 3 bars of pressure.

Furthermore, we tested two samples of aluminum with a thickness of 500 μm. A dome made of aluminum with that thickness will be used to cover the container for the deuterium crystal in the PSI UCN source. The goal of that measurement was to find out whether there is a visible difference in UCN transmission between aluminum that was solely cleaned with alcohol
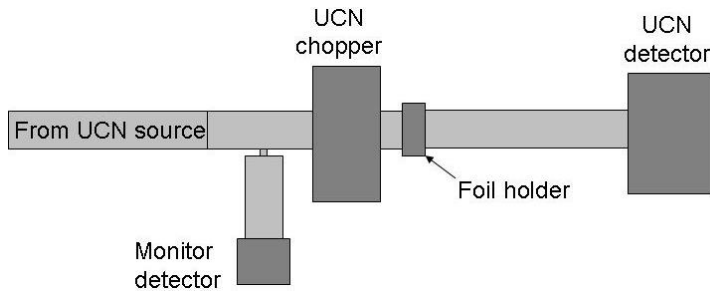
Figure 6.1: Setup for the determination of UCN transmission of foils.

and demineralized water and aluminum cleaned in an ultra-sonic bath before being rinsed with demineralized water. The ultra-sound treatment has been observed to erode the foils irregularly.

Finally we also measured the UCN transmission of the aluminum foil used as entrance window for the Cascade-U detector. As many measurements were done with that detector, it is important to know that value. In case of the foil transmission measurements, the results are relative to each other, i.e., it is not necessary to know the absolute detection efficiency, the efficiency just has to be constant.

6.1 Measurement Principle

The setup (sketched in Fig. 6.1) is similar to the transmission measurement using the TOF method. The UCN pass the monitor detector before entering the chopper. The chopped beam propagates through UCN guides and a foil holder before reaching the UCN detector. The measurement is done twice, once with and once without a foil in the holder. The UCN transmission of the foil is found by comparing these two TOF spectra (also in [22]).
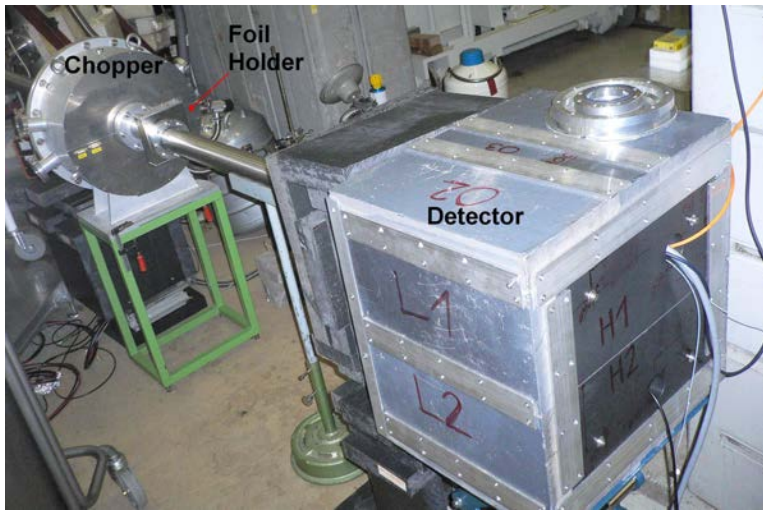
99

Figure 6.2: Setup for the measurement of UCN transmission of foils.

6.2 Lab Situation

The transmission of foils was measured in a setup using a special foil holder. This holder makes it possible to measure the UCN count rate with a defined setup, with and without a foil in the beam line, without altering anything else in the geometry. The holder is a vacuum tight stainless steel container with flanges on the front and the back, to connect UCN guides. There is an insert in the container allowing fixation of a foil in the beam line. The insert is made to minimize the area of slits between guide and foil.

Measurements were done with the foil holder mounted at two different positions, directly behind the chopper and in front of the detector. The analysis did not show a significant difference between the two positions.
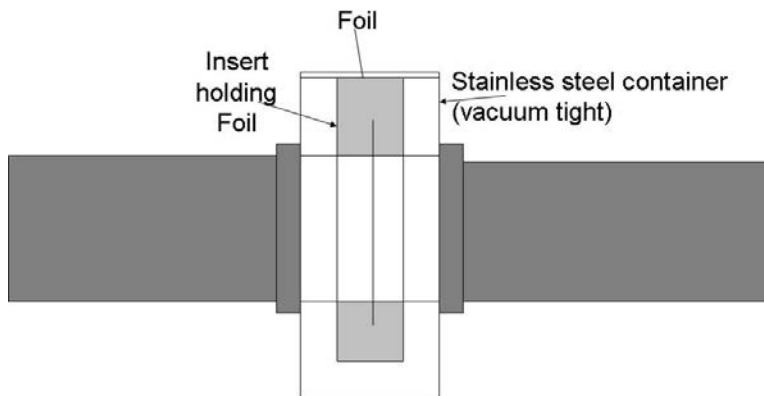
Figure 6.3: Schematic of the foil holder used in the experiments.

6.3 Analysis

The analysis of foil transmission measurements is similar to the analysis of the TOF measurements. However, it is much simpler, as the setup is identical for both measurements and only a foil is inserted. This means that the length of the setup is constant. Hence, we can express all the systematic uncertainties as errors on the velocity bounds, which logically reduces the relative errors between the different foil measurements. Therefore, the statistics are clearly the dominating uncertainty.

6.4 Results

Using the same analysis makro as described in the TOF section, we get the results shown in table 6.1 (p.102) for the tested foils.

Foil	Thickness [μm]	lower integration limit [m·s^{-1}]	upper integration limit [m·s^{-1}]	Transmission
AlMg3	100	3.3±0.04	6±0.13	0.72±0.01
Al6061	100	3.3±0.05	6±0.08	0.67±0.01
Al3003	100	3.3±0.04	6±0.13	0.73±0.01
Cascade-U	100	3.3±0.04	6±0.13	0.57±0.01
TK1 - AlMg3	500	5±0.11	9±0.33	0.56±0.01
TK2 - AlMg3	500	5±0.11	9±0.33	0.53±0.01

Table 6.1: Transmission values for the measured foils.

The transmission of the 100 μm AlMg3 foil and the Al3003 are comparable, however, AlMg3 was superior to Al3003 in a burst-pressure test [21]. The end window of the PSI UCN source, will probably be made of AlMg3.

The two tested pieces of 500 μm AlMg3 (TK1, TK2) have transmission values that almost agree within the error (TK2 was treated with ultrasound). Therefore, if necessary, the aluminum dome for the deuterium container can be treated with ultra-sound in order to reduce the amount of dirt on its surface, the caused UCN loss would be small.

The Cascade-U foil has a low UCN transmission, the Cascade company has been informed about that and they have decided to change the aluminium foil used as a substrate for the boron layer in their detectors.

6.4.1 Comparison with Literature Values

The PSI UCN group has done similar measurements with thin foils at ILL in 2004. The results for the UCN transmission of the AlMg$_3$ foil are in good agreement with the values obtained here. However, the theoretical prediction made for the transmission that were made in 2004, significantly deviated from the experimental results. The theory predicted much higher transmission and the reason for this deviation was a topic of further research.

One suspicion was that the foils were contaminated with a strongly UCN

absorbing material, e.g. boron, cadmium, or gadolinium. The Mainz UCN group conducted further research and employed a large variety of material analysis methods on samples of the foils measured at ILL. Among the methods were neutron activation and different methods of inductively coupled plasma spectroscopy. However, the analysis showed no UCN absorber admixture, large enough to explain the deviations, to any of the samples. The reason for the deviation is still puzzling and has not yet been resolved. One reason, still to be confirmed, could be the surface roughness of the foils. If the transmission of a foil is calculated using quantum mechanics and a model for the roughness of the foil, results might match the experimental data. The analysis is still ongoing.

Chapter 7

Storage Experiments

Storage experiments to characterize the UCN guides will be set up similarly to the pre-storage measurements described above. The difference is that the pre-storage is a mean of shaping the spectrum and the storage measurement stores the UCN in the vessel that is to be characterized.

The guide to be characterized is mounted in between two DLC coated VAT valves. This reactor will be operated in pulsed mode to maximize the number of stored UCN. As soon as the incoming and out-going neutron flux have equal magnitudes, shutter 1 is closed and then the trapping time - which is a fixed value in the pre-storage experiment - is varied from 1 second to the maximum trapping time, i.e., when the opening produces no significant signal anymore because all UCN are either lost or have decayed.

Storage experiments are not sensitive to surface roughness in the storage volume. However, in a storage experiment great care has to be invested in the elimination of slits in the storage volume.

For technical reasons, we were not able to perform a storage measurement with a setup like the one that will be used for the final guide characterization.
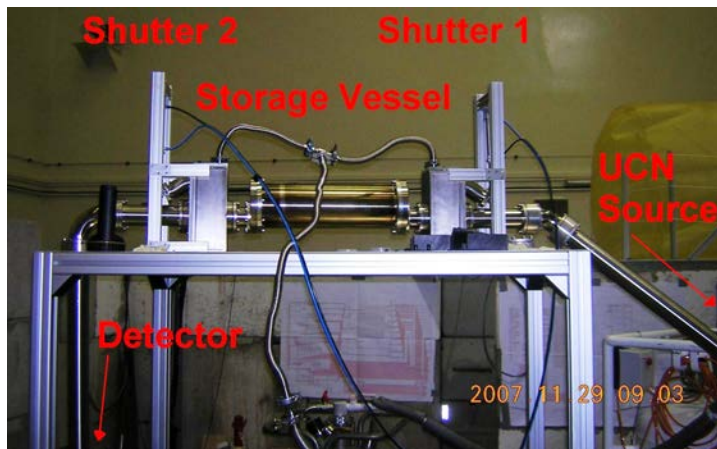
Figure 7.1: Storage experiment carried out by the PSI UCN group in Mainz, November 2007.

Within this thesis, hardware preparations for storage measurements were done (section 3.3), but due to lack of beam time, no storage measurements could be performed.

Chapter 8

Summary and Conclusions

This thesis concentrates on the hardware preparation, performance, and analysis of transmission measurements of UCN guides.

An electronic system was designed and built that remotely controls shutters necessary to perform different types of pre-storage and storage measurements. The system can be operated manually or via USB by computer.

In a comparative study, transmission values for stainless steel and glass UCN guides were obtained. Furthermore, UCN transmission through different types of aluminum foils was investigated. Consequently, it was decided to use NiMo coated, hand-washed glass tubes as UCN guides and $AlMg_3$ as end window for the UCN guides at PSI. However, R&D in the field of UCN guides is still ongoing, as to provide even better UCN guides.

In this work, we have used two different types of transmission measurements, via time-of-flight and via pre-storage. These types of measurements directly lead to different sensitivities towards UCN which undergo specular or diffuse reflection. Hence, we defined the direct transmission as a measure of the transmitted, specularly reflected UCN. One has to keep this in mind, when comparing to literature values of transmission. The total transmission

of a guide cannot be calculated from direct transmission measurements, but a high direct transmission is important for a fast filling of future experiments.

The transmission of the 100 μm AlMg$_3$ foil, was found to be 0.72±0.01. The direct transmission of the best glass test guide was found to be 0.82±0.01±0.04. Using these values and a total guide length of 8 m for a typical UCN guide system at PSI, the direct transmission through that length is ∼0.15, including the end window foil. This assumes the transmission of the stainless steel parts in the guide setup to be similar to the glass guide, as their transmission has not been measured yet. The validity of this assumption can be seen by comparing the Nocado and the glass guide results.

The obtained transmission value seems low but one has to clearly point out that it includes only the *direct* transmission. It is not yet possible, to calculate the total transmission of the guide system from experimental data, as pre-storage measurements still have to be done with a good sample tube.

The analysis of our data lead to the conclusion that pre-storage and TOF measurements can be used as complementary measurements of the UCN transmission of guides, both having advantages and disadvantages.

The TOF measurement is limited by the accuracy on the chopper offset δt and by the fact that the integration boundaries should be placed on positions in the TOF spectrum with a small slope.

Our pre-storage measurements are mostly limited by the fact, that the UCN spectrum leaving the pre-storage vessel is not accurately known and has to be simulated, by the uncertainty of the reactor pulse power and by statistics which however, could easily be improved by measuring more pulses.

Bibliography

[1] F. Atchison, M. Baumann, B. Blau, K. Bodek, B. van den Brandt, M. Daum, R. Dlling, P. A. Duperrex, A. Fuchs, P. Geltenbort, D. George, W. Gloor, S. Grigoriev, P. Hautle, G. Heidenreich, F. Heinrich, R. Henneck, S. Heule, Th. Hofmann, M. Horvat, F. Jenni, St. Joray, M. Kasprzak, K. Kirch, A. Knecht, J. A. Konter, M. Kuzniak, Ch. Perret, A. Pichlmaier, D. Rebreyend, R. Reiser, U. Rohrer, S. Teichmann, M. Wohlmuther, G. Zsigmond, J. Zuellig, *Proceedings of the International Collaboration on Advanced Neutron Sources*, ICANS-XVIII, Guangdong, China, 2007.

[2] A. Anghel, F. Atchison, B. Blau, K. Bodek, B. van den Brandt, M. Daum, R. Dlling,M. Dubs, P. A. Duperrex, A. Fuchs, P. Geltenbort, D. George, L. Göltl, S. Grigoriev, P. Hautle, G. Heidenreich, F. Heinrich, R. Henneck, S. Heule, H. Heyck, Th. Hofmann, St. Joray, M. Kasprzak, K. Kirch, S. Kistryn, A. Knecht, J. A. Konter,T. Korhonen, M. Kuzniak, B. Lauss, A. Mezger, A. Mtchedlishvili, G. Petzoldt, A. Pichlmaier, C. Plonka, R. Reiser, U. Rohrer, S. Teichmann, K. Thomsen, W. Wagner, M. Wohlmuther, G. Zsigmond, J. Zuellig, and J. Zmeskal,*The PSI Ultracold Neutron Source*, International Workshop on Particle Physics with Slow Neutrons, ILL, Grenoble, 28-31 May 2008,

acc. for publ. in Nucl. Instr. and Meth. in Phys. Res. A.

[3] M. Wohlmuther, G. Heidenreich, *The spallation target of the ultra-cold neutron source UCN at PSI*, Nucl. Instr. and Meth. in Phys. Res. A 564, 51 (2006).

[4] A. P. Serebrov, V. A. Mityukhlyaev, A. A. Zakharov, T. Bowles, G. Greene, and J. Sromicki,*Solid deuterium source of ultracold neutrons based on a pulsed spallation source*, JETP Letters, Volume 66, Number 12 / Dezember 1997.

[5] A. Steyerl, H. Nagel, F.X. Schreiber, K.A. Steinhauser, R. Gahler, W. Glser, P. Ageron, J.M. Astruc, N. Drexel, R. Gervais and W. Mampe, *A new source of cold and ultracold neutrons*, Physics Letters A, 116 (1986), p.347.

[6] F. Atchison, P. Baumanna, T. Brys, M. Daum, A. Egorov, P. Fierlinger, P. Fuchs, R. Henneck, St. Joray, R. Keil, K. Kirch, R. Krutova, G. Khne, V. T. Lebedev, H. Obermeier, D. N. Orlova, Ch. Perret, A. Pichlmaier, Ph. Richard, A. Serebrov, and S. Thies, *On the use of lead/tin alloys as target material for the production of spallation neutrons*, Nucl. Instr. and Meth. in Phys. Res. A 539, 646 (2005).

[7] D. Anicic, M. Daum, G. Dzieglewski, D. George, M. Horvat, G. Janser, F. Jenni, I. Jirousek, K. Kirch, T. Korhonen, R. Knzi, A. Mezger, U. Rohrer and L. Tanner, *A fast kicker magnet for the PSI 600 MeV proton beam to the PSI ultra-cold neutron source*, Nucl. Instr. and Meth. in Phys. Res. A 541, 598 (2005).

[8] A. Frei, Yu. Sobolev, I. Altarev, K. Eberhardt, E. Gutsmiedl, R. Hackl, G. Hampel, F. J. Hartmann, W. Heil, J. V. Kratz, Th. Lauer,A. Lizon

109

Aguilar, A. R. Müller, S. Paul, Yu. Pokotilovski, W. Schmid, L. Tassini, D. Tortorella, N. Trautmann, U. Trinks, and N. Wiehl, *First production of ultracold neutrons with a solid deuterium source at the pulsed reactor TRIGA Mainz*, The European Physical Journal A 34, 119-127 (2007).

[9] I. Altarev, M. Daum, A. Frei, E. Gutsmiedl, G. Hampel, F. J. Hartmann, W. Heil, A. Knecht, J. V. Kratz, T. Lauer, M. Meier, S. Paul, U. Schmidt, Y. Sobolev, N. Wiehl, and G. Zsigmond, *Neutron velocity distribution from a superthermal solid $^2H_2$ ultracold neutron source*, The European Physical Journal A - Hadrons and Nuclei, DOI 10.1140/epja/i2008-10604-8.

[10] R. Golub, D Richardson, S.K. Lamoreaux, *Ultra-Cold Neutrons*, IOP Publishing Ltd 1991 (Adam Hilger).

[11] W.-M.Yao *et al.* (Particle Data Group), J. Phys. G 33, 1 (2006) and 2007 partial update for the 2008 edition.

[12] B. Povh, K. Rith, C. Scholz, F. Zetsche, *Particles and Nuclei, An Introduction to the Physical Concepts*, Fourth edition, Springer 2003.

[13] Ullrich Uwer, *Vorlesung Physik V, Teilchen und Kerne*, Transparencies from his Homepage: `http://www.physi.uni-heidelberg.de/~uwer/lectures/PhysikV/vorlesung.html`.

[14] S. Heule, *Production, Characterization and Reflectivity Measurements of Diamond-like Carbon and other Ultracold Neutron Guide Materials*, Phd. Thesis, University of Zrich, 2008.

[15] Siemens AG, Industrial Automation Systems, LOGO! Manual `http://cache.automation.siemens.com/dnl/DM2MDIzMwAA_16527461_HB/Logo_e.pdf`.

[16] Homepage of the Cascade group, `www.n-cascade.com`.

[17] P. Fierlinger, A. Pichlmaier, H. Rauch, *A time-of-flight chopper for ultra-cold neutrons*, Nucl. Instr. and Meth. in Phys. Res. A 557 (2006) 572-575.

[18] K. Eberhardt, A. Kronenberg, *Der Forschungsreaktor TRIGA Mainz - Eine Neutronenquelle für vielseitige Anwendungen in Forschung und Lehre*, Kerntechnik 65, 263 (2000).

[19] G. Hampel, K. Eberhardt, and N. Trautmann, *The research reactor TRIGA Mainz*, Int. J. for Nucl. Power, ISSN 1431, atw 5 (2006).

[20] Internal memo, Geza Zsigmond.

[21] PSI UCN-Group internal memo, L. Göltl and R. Knecht, *Berstversuche März 2008*.

[22] F. Atchison, B. Blau, M. Daum, P. Fierlinger, P. Geltenbort, M. Gupta, R. Henneck, S. Heule, M. Kasprzak, A. Knecht, M. Kuzniak, K. Kirch, M. Meier, A. Pichlmaier, R. Reiser, B. Theiler, O. Zimmer, and G. Zsigmond, *Measurement of the Fermi potential of diamond-like carbon and other materials* Nucl. Instr. and Meth. in Phys. Res. B 260, 647 (2007).
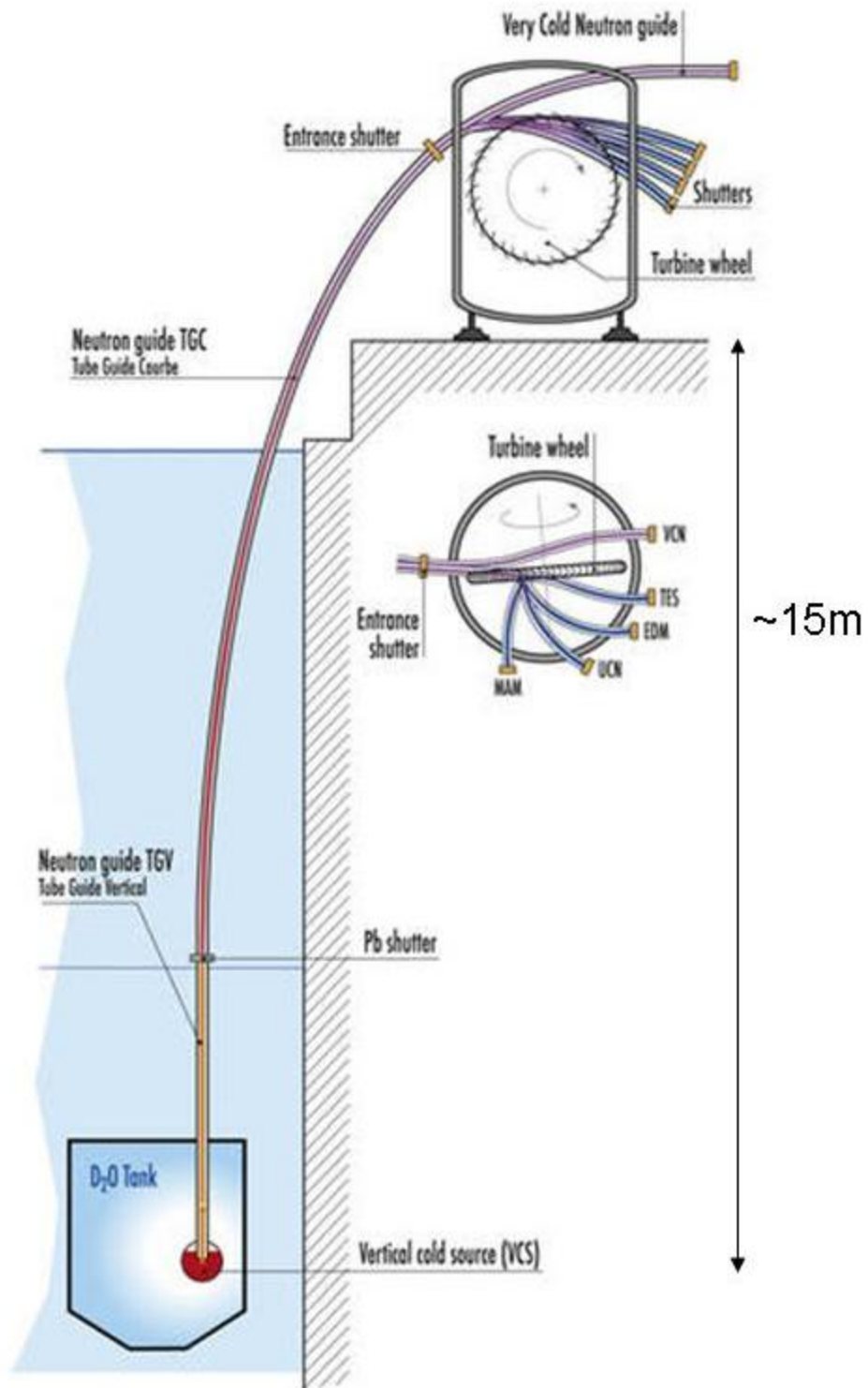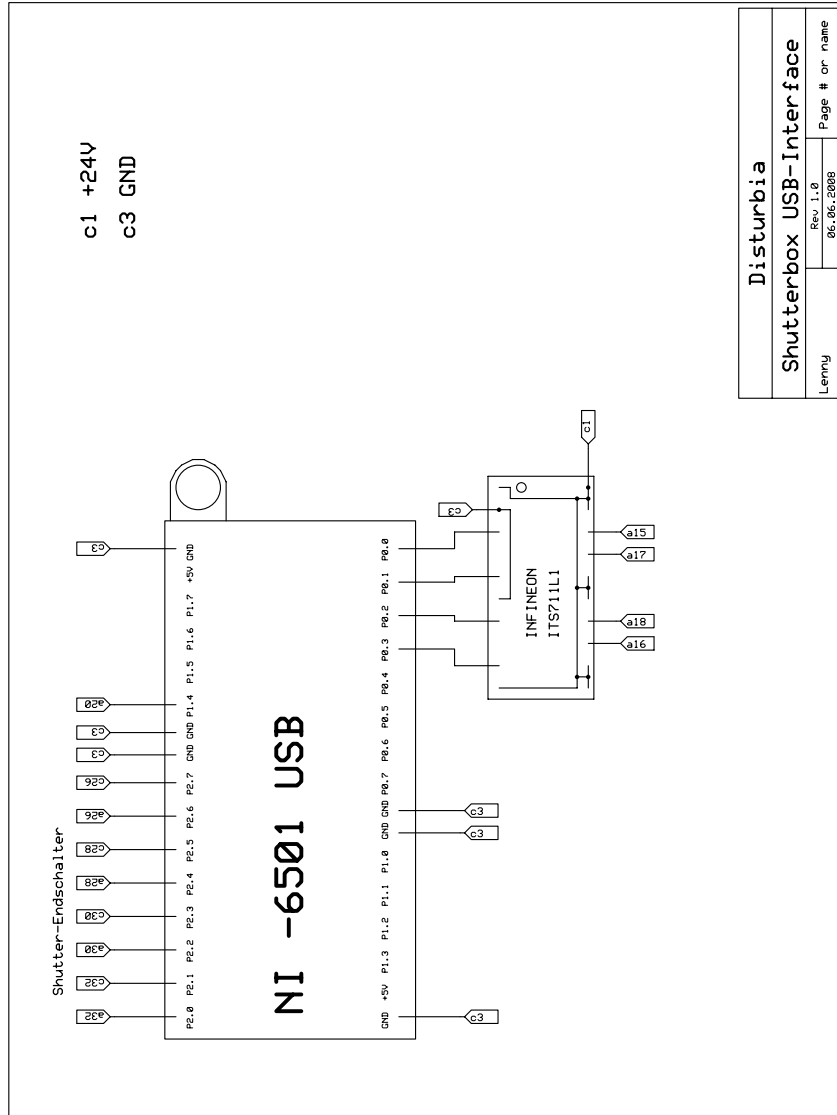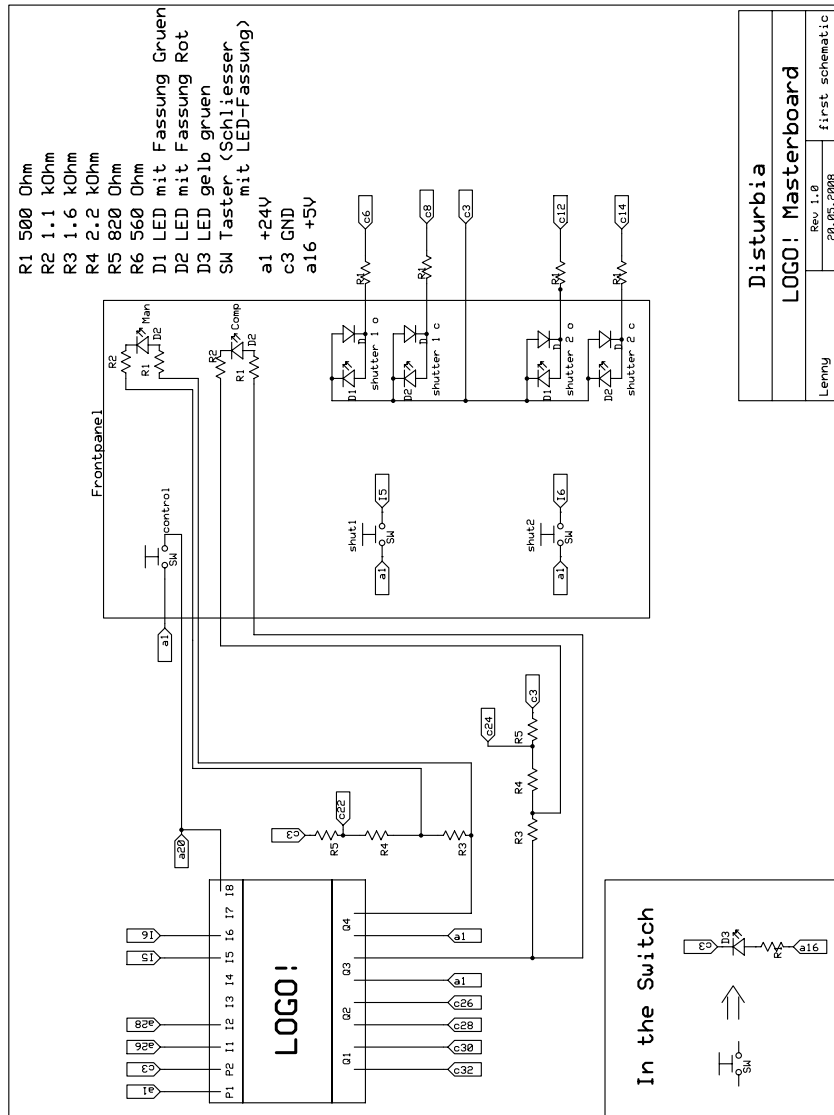
Chapter 9

Appendix

Appendix

Figure A1: Steyerl type turbine used to produce UCN at the Institut Laue Langevin in Grenoble www.ill.eu/pf2.

Figure B1: Schematic for NI board.

Figure B2: Schematic for the master board.

R1 500 Ohm
D1 LED mit Fassung Gruen
D2 LED mit Fassung Rot
D3 LED gruen gelb
SW Taster (schliessermit LED-Fassung)

a1 +24V
c3 GND
a16 +5V

Frontpanel

LOGO!

In the Switch

Disturbia
LOGO! Slaveboard

Rev 1.0
20.05.2008

first schematic

Lenny
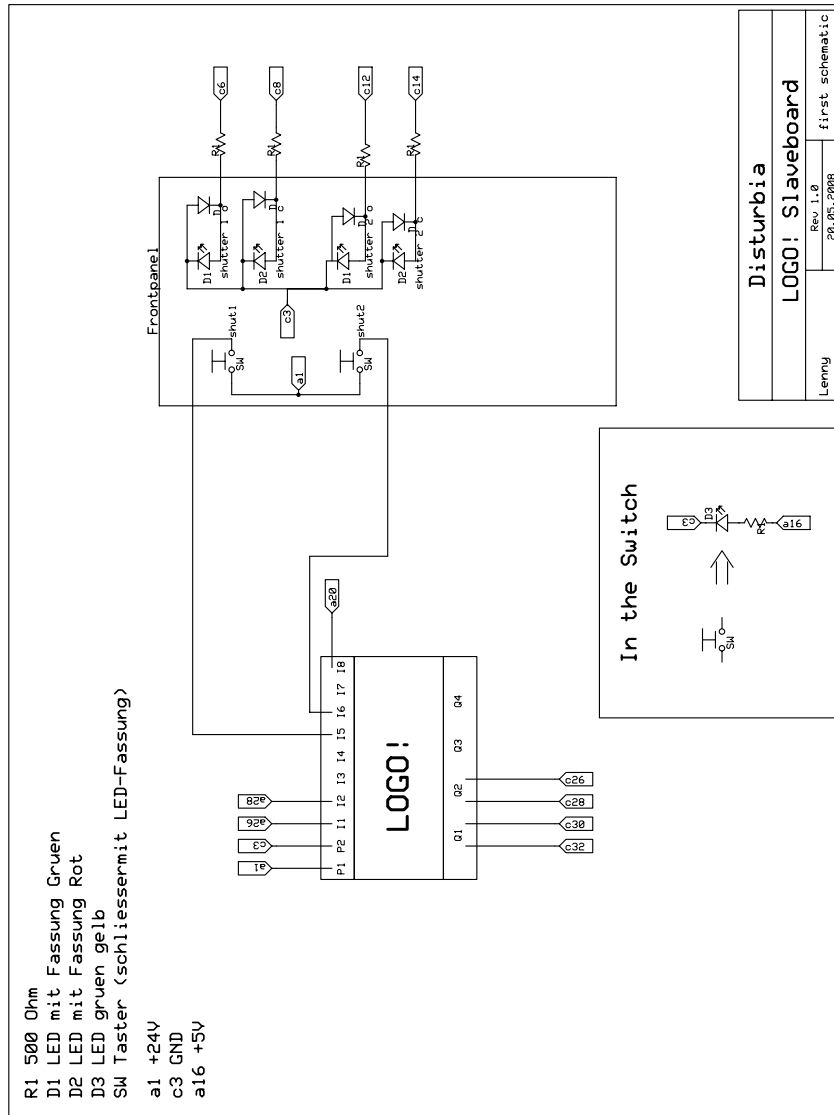
Figure B3: Schematic for the slave board.

shutter

Endschalter (zu)

GND

Ventil

+24V

Endschalter (auf)

Disturbia

Shutter (verkabelung)

| Lenny | Rev 1.0 16.06.2008 | kabel |
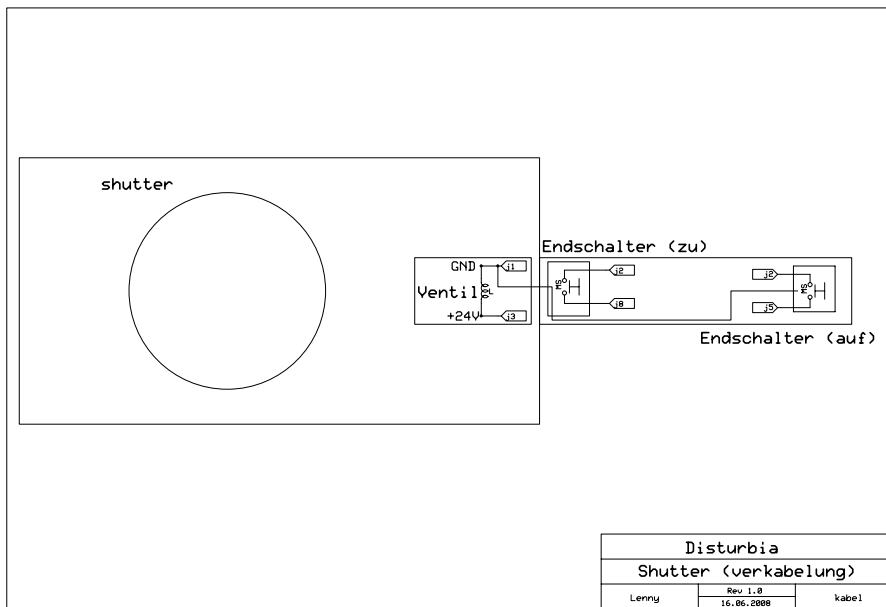
Figure B4: Schematic for the shutter, i.e., the connections to the end position switches and the control valve.
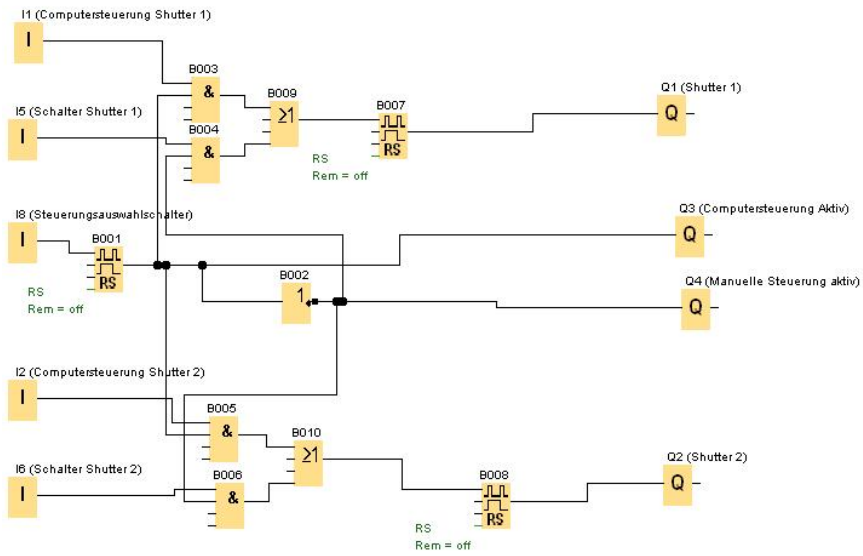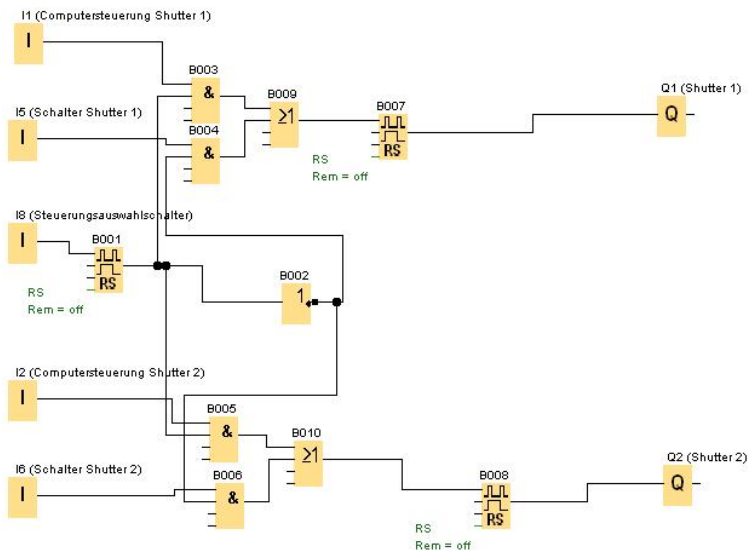
Figure B5: Schematic for the LOGO! on the master board.

Figure B6: Schematic for the LOGO! on the slave board .